DTIC FILE COPY

AD-A231 836

Contract No. F49620-85-C-0080

"Unsteady Behavior of Turbulent Shear Flows"

Co-Principal Investigators:
Ho, Chih-Ming
P. Huerre
L. G. Redekopp

Department of Aerospace Engineering
University of Southern California
Los Angeles, California 90089-1191

July 25, 1990

Final Technical Report
Period: May 01, 1985 to April 30, 1990

DTIC
ELECTE
FEB 15 1991
S B D

Air Force Office of Scientific Research
Bolling Air Force Base
Washington, D.C. 20332-6448

DISTRIBUTION STATEMENT A
Approved for public release
Distribution Unlimited

REPORT DOCUMENTATION PAGE

Form Approved
OMB No. 0704-0188

Public reporting burden for this collection of information is estimated to average 1 hour per response, including the time for reviewing instructions, searching existing data sources, gathering and maintaining the data needed, and completing and reviewing the collection of information. Send comments regarding this burden estimate or any other aspect of this collection of information, including suggestions for reducing this burden, to Washington Headquarters Services, Directorate for Information Operations and Reports, 1215 Jefferson Davis Highway, Suite 1204, Arlington, VA 22202-4302, and to the Office of Management and Budget, Paperwork Reduction Project (0704-0188), Washington, DC 20503.

1. AGENCY USE ONLY (Leave blank)	2. REPORT DATE	3. REPORT TYPE AND DATES COVERED
	25 July 1990	FINAL REPORT 1 May 85 TO 30 Apr 90

4. TITLE AND SUBTITLE

Unsteady Behavior of Turbulent Shear Flows

5. FUNDING NUMBERS

F49620-85-C-0080

PE - 61102F
PR - 2307
TA - A2

6. AUTHOR(S)

Chih-Ming Ho, P. Huerre, L. G. Redekopp

7. PERFORMING ORGANIZATION NAME(S) AND ADDRESS(ES)

Dept of Aerospace Engineering
University of Southern California
Los Angeles, CA 90089-1191

8. PERFORMING ORGANIZATION REPORT NUMBER

AFOSR-TR- 91 0010

9. SPONSORING/MONITORING AGENCY NAME(S) AND ADDRESS(ES)

AFOSR/NA
Building 410
BOLLING AFB, DC 20332-6448

10. SPONSORING/MONITORING AGENCY REPORT NUMBER

F49620-85-C-0080

11. SUPPLEMENTARY NOTES

12a. DISTRIBUTION/AVAILABILITY STATEMENT

Approved for public release;
distribution is unlimited

12b. DISTRIBUTION CODE

13. ABSTRACT *(Maximum 200 words)*

Theoretical studies on the temporal and spatial structure in blunt-body wakes have revealed the necessary conditions under which global, self-sustained oscillations appear and have provided firm criteria for specifying the frequency of these oscillations. The theory has also bveen employed to describe the preferred mode in jets. In addition, a theoretical description of the appearance of the spatial chaos in wake-shear layers, and its representation in terms of a one-dimensional map, has been provided. An experimental facility annd necessary instrumentation have been assembled and experiments are in progress on spatial chaos in wake-shear layers. Preliminary results have revealed a parameter domain where a temporal vascillation accurs between the Karman wake mode and the shear layer mode.

14. SUBJECT TERMS

Turbulence, Shear flow, Chaos, Instability

15. NUMBER OF PAGES

19

16. PRICE CODE

17. SECURITY CLASSIFICATION OF REPORT	18. SECURITY CLASSIFICATION OF THIS PAGE	19. SECURITY CLASSIFICATION OF ABSTRACT	20. LIMITATION OF ABSTRACT
UNCLASSIFIED	UNCLASSIFIED	UNCLASSIFIED	UL

91 2 12 033

UNSTEADY SEPARATION AND UNSTEADY SHEAR LAYERS
(Task 2)

Principal Investigator: Ho, Chih-Ming

ABSTRACT

The process of engulfing fluids from two streams into the shear region is one of the most important technical problems in fluid mechanics research. A new entrainment mechanism, unsteady azimuthal deformation was identified to be more effective than vortex merging in a two-dimensional flow. This mechanism can make the homogeneous elliptic jet entrain twice the mass than a circular jet. During this contract period, the effect of temperature on the evolution of the three-dimensional jet was studied.

ACCOMPLISHMENTS

The results are briefly summarized here. The detailed information can be found in the attached papers or in the publication list.

Application of High Entrainment of Elliptic Jets

(Ref. Ho, Austin and Hertzberg, Proc. Asian Fluid Mech. Congress)

The high entrainment of a jet issuing from an elliptic nozzle has been applied in ramjet combustor and in supersonic jets. The data showed significant improvements in mixing.

Stability Analysis of an Elliptic Jet

(Ref. Koshigoe, Ho and Tubis, AIAA paper No. 87–2733
Koshigoe, Tubis and Ho, Phys. Fluids, 1988)

The azimuthal deformation of the vortices is produced by the self-induction of the asymmetric distribution of vorticity in a structure. The vortex distortion depends on the stability process. Both the amplification rate and the phase speed are functions of the azimuthal vorticity distribution and they also vary with the temperature. When a temperature gradient exists across the velocity shear with different thickness around the nozzle, the differences in the growth rate and the phase speed around the nozzle is amplified. Hence, the deformation of the vortices is accentuated by the temperature gradient and the entrainment is expected to be modified.

The Hot Jet Facility

We intend to operate the jet in the speed region where the compressibility effect is appreciable and in the temperature range which is much higher than the room temperature. Many versions of the modification have been carried out. We were able to increase the jet Mach

number to about 0.2, 230 ft/sec, by installing three additional blowers. The maximum operating temperature is about 500°F. The temperature in the stagnation and at exits of the heaters are monitored by thermistors.

Flow Visualization

There is an appreciable density fluctuation in the hot jet. We then can visualize the entrainment process in the hot elliptic jet. A shadowgraph and a Schlieren system were set up for this purpose. A spark-type light source with micro second duration was used. The frequency of the light pulse was controlled by the trigger signal and could be varied from a single pulse up to 1 kHz. We adjusted the pulse rate to match the frame rate of the video camera and took a movie of the hot jets.

The shadowgraph showed that the initial boundary layer is laminar and vortices roll up at a downstream location. The spreading in the plane containing the minor axis spreads much faster than in the major axis plane. This is consistent with the measurements. We did not observe the side jets caused by the absolute instability (Bechert et al., 1988) in either the still picture or the video movie.

Temperature Fluctuations

The maximum temperature of the jet can reach 500°F. To hold and operate a hot-wire in a flow of this high temperature is not a trivial job. The time spent in solving this problem was more than we expected. We need to find a specially high temperature solder to attach the platinum wire to the steel prongs. The probe body also requires temperature resistance because part of the probe is inside the flow. The calibration procedures have been established. The time constant of the wire and the digital frequency compensation technique were accomplished. The frequency response was extended from 150 Hz to 3000 Hz.

The pdf of temperature fluctuations was measured along the major and the minor axes at several streamwise locations. When the pdf was compared at corresponding radial locations in the major and minor axis planes, an interesting feature was found; the pdf in the minor axis plane was being skewed toward the low temperature side. This result reconfirms the fact that entrainment of the ambient cold near the minor axis region is more pronounced. The standard deviation of the pdf indicates the level of temperature fluctuations. The standard deviations in the minor axis plane are always higher than those in the major axis plane.

COPY INSPECTED

KEYNOTE TALKS IN CONFERENCES

1. "Fundamental Aspects of Unsteady Separation", AFOSR Super Maneuverability Initiative Meeting, Boulder, Colorado, March 11, 1985.

2. "Entrainment and Turbulence Structures", 22nd JANNAF Combustion Meeting, Pasadena, California, October 11, 1985.

3. "Evolution of Coherent Structures and Small Scale Transition in Mixing Layers", Workshop on Computational Fluid Mechanics, Institute of Nonlinear Science, University of California at Davis, Davis, California, July 18, 1986.

Availability Codes
Avail and/or
Dist Special
A-1

4. "Vortex Evolution and Turbulence Control", 24th JANNAF Combustion Meeting, Monterey, California, October 5–9, 1987.

5. "Vortex Dynamics of Unsteady Flows", First National Fluid Dynamics Congress, Cincinnati, Ohio, July 23–25, 1988.

PH.D. THESIS

1. "Small Scale Transition and Preferred Mode in an Initally Laminar Plane Jet" by F. B. Hsiao.

2. "The Unsteady Aerodynamics of a Plunging Airfoil" by S. H. Chen.

PUBLICATIONS

1. "Unsteady Separation in a Boundary Layer Produced by an Impinging Jet", with Didden, N., *J. Fluid Mech.*, Vol. 160, pp. 235–256, 1985.

2. "Near-Field Pressure Fluctuations of an Elliptical Jet", with Gutmark, E., *AIAA Journal*, Vol. 23, pp. 354–358, 1985.

3. "An Alternative Look at the Unsteady Separation Phenomenon", *Recent Advances in Aerodynamics*, ed. Krothapalli, A. and Smith, C. A., pp. 165–178, Springer, 1985.

4. "Vortex Pair behind a 3-D Backward Facing Step", with Shih, C., *Bulletin of the American Physical Society*, Vol. 30, p. 1701, 1985.

5. "Unsteady Aerodynamics of a Plunging Airfoil", with Cheng, S. H., *Bulletin of the American Physical Society*, Vol. 30, p. 1697, 1985.

6. "Unsteady Separation on Elliptic Cylinder", with Shih, C., *Bulletin of the American Physical Society*, Vol. 31, p. 1708, 1986.

7. "Visualization of a Forced Elliptic Jet", with Gutmark, E., *AIAA Journal*, Vol. 24, pp. 684–685, 1986.

8. "Interactions between Large Structures and Small Eddies in a Plane Jet", with Hsiao, F. B., IUTAM Symposium on Fluid Mechanics in the Spirit of G. I. Taylor, 1986.

9. "Aerodynamics Research on Flow Separation and Dynamic Stall: Some Recent Advances", with Cheng, H. K., *Aerospace Simulation*, ed. M. Ung, pp. 187–198, 1986.

10. "Near-Wake of an Unsteady Symmetric Airfoil", with Chen, S. H., *J. of Fluids and Structures*, Vol. 1, pp. 151–164, 1987.

11. "Vortex Induction and Mass Entrainment in a Small Aspect Ratio Elliptic Jet", with Gutmark, E., *J. Fluid Mech.*, Vol. 179, pp. 383–405, 1987.

12. "Application of a Generalized Shooting Method to the Linear Instability Analysis of Elliptic Core Jets", with Koshigoe, S. and Tubis, A., AIAA paper No. 87–2733, 1987.

13. "Vortex Deformation in Elliptic-Core Jets from the Perspective of Linear Instability Analysis", with Koshigoe, S. and Tubis, A., *Phys. of Fluids*, Vol. 31, pp. 2504–2517, 1988.

14. "Evolution of Coherent Structures", Conference on Turbulence Structures in Free Shear Flows and their Detection by Proper Orthogonal Decomposition, Newport, Rhode Island, 1988.

15. "Entrainment of Asymmetric Jets", with Austin, T., AFOSR Turbulence Research Contractors' Meeting, 1988.

16. "Global Oscillations in Helium Jets", with Guyon, E., Huerre, P. and Monkewitz, P. A., *Bulletin of the American Physical Society*, Vol. 33, p. 2233, 1988.

17. "Temperature Effects on Entrainment of an Elliptic Jet", with Austin, T., *Bulletin of the American Physical Society*, Vol. 33, p. 2237, 1988.

18. "Entrainment of 3-D Shear Layers", with Austin, T. and Hertzberg, J., The Fourth Asian Congress of Fluid Mechanics, Hong Kong, 1989.

Vortex deformation in elliptic-core jets from the perspective of linear instability analysis

Shozo Koshigoe
Code 3892, Naval Weapons Center, China Lake, California 93555-6001

Arnold Tubis
Department of Physics, Purdue University, West Lafayette, Indiana 47907

Chih-Ming Ho
Department of Aerospace Engineering, University of Southern California, Los Angeles, California 90089

(Received 10 August 1987; accepted 17 May 1988)

An attempt is made to identify the underlying mechanisms for the deformation of coherent structures that occurs in the initial state of axis switching of elliptic-core jets. The generalized shooting method is applied to jets with elliptic-core regions of constant flow. The analysis shows that there are three conditions on groups of eigenmodes of elliptic-core jets which are necessary for the deformation. They are (1) proper localizations without excessive overlapping; (2) sufficiently large phase-speed differences; and (3) comparable spatial amplification rates. The qualitative behaviors of elliptic-core jets in relation to these three conditions are studied with respect to independent and joint variations of core eccentricity, azimuthal distribution of momentum thickness, and compressibility.

I. INTRODUCTION

Jets are generic configurations in many engineering devices, e.g., ramjet combustors, and they therefore have attracted attention from numerous researchers. Understanding the entrainment mechanism and developing control techniques are the key research goals in jet studies. More than a decade ago, effort was concentrated on investigating small random eddies, but success was limited. Since the evolution of large coherent structures[1] was recognized to be the mechanism that determined the mass transfer between streams, progress has been very much accelerated. Many active-control[2–4] as well as passive-control[5] techniques have been developed for manipulating the entrainment process. The basic control principle is to enhance the unsteady distortion of structures and thereby induce large amounts of mass to move across the shear layer. Passive control is especially interesting, because no additional energy is required. In the case of the elliptic nozzle used by Ho and Gutmark,[5] the entrainment can be approximately ten times higher than that for a two-dimensional (2-D) axisymmetric or plane jet. Schadow and Gutmark[6] tested this type of passive control in a ramjet combustor and found significant improvement in the combustion efficiency.

Instability analysis offers a great deal of insight into the development of free shear layers. Many properties of the coherent structures in a 2-D flow can be predicted from instability calculations. Even experiments in turbulent mixing layers[7] have demonstrated that fine details of the eigenfunctions can be well determined from the analysis. Crighton[8] examined the instability of an elliptic vortex-sheet jet. However, the vortex-sheet approximation is only valid for low wavenumbers. In the three-dimensional (3-D) elliptic-jet case, new features, e.g., aspect ratio and distribution of the momentum thickness, are introduced into the problem and provide a new domain of applicability of instability calculations to the design of passive controls. There are four classes of instability modes for elliptic-core jets.[9,10] Furthermore, a calculation scheme more general than that used in 2-D cases[11] is needed to handle the nonseparable boundary value problem.

One of the most peculiar aspects of elliptic-core jets is axis switching,[12] which is of interest from a fundamental scientific point of view and for its potential applications. The initial development of axis switching is characterized by the deformation of coherent structures. This deformation can be associated with the self-induction of the asymmetrical distribution of vorticity in the jet, which causes differences in rollup locations. The portions of the elliptic-jet vortical structures near the major axis roll up slightly further downstream from those near the minor axis. Thus the overall pattern of rolled up structure is deformed. This deformation in the elliptic jet is clearly seen in the forced elliptic jets in the paper[5] of Ho and Gutmark (see Fig. 1). The analysis of the complete evolution of axis switching is beyond the scope of the present work. However, without the deformation of the initial large-scale-structure development as just described, there would be no axis switching.

In this paper, we analyze the spatial instability modes of elliptic-core jets in order to demonstrate the essential underlying mechanisms which cause the initial vortex deformation. The generalized shooting method,[13] based on both integral and differential equations, is used for the calculations since it has been found to be more practical to apply than the Helmholtz integral equation formulation.[9] Some of the formal and numerical aspects of calculations are reviewed in Sec. II for convenience of discussion in the later sections. (For more details, see Ref. 13.) In Sec. III, the instability modes for incompressible flows are studied as the limit of compressible flows in order to clearly assess the effects of compressibility later in Sec. IV.

Three conditions on groups of eigenmodes are identified as necessary for vortex deformation in elliptic-core jets.

 0031-9171/88/092504-14$01.90 © 1988 American Institute of Physics

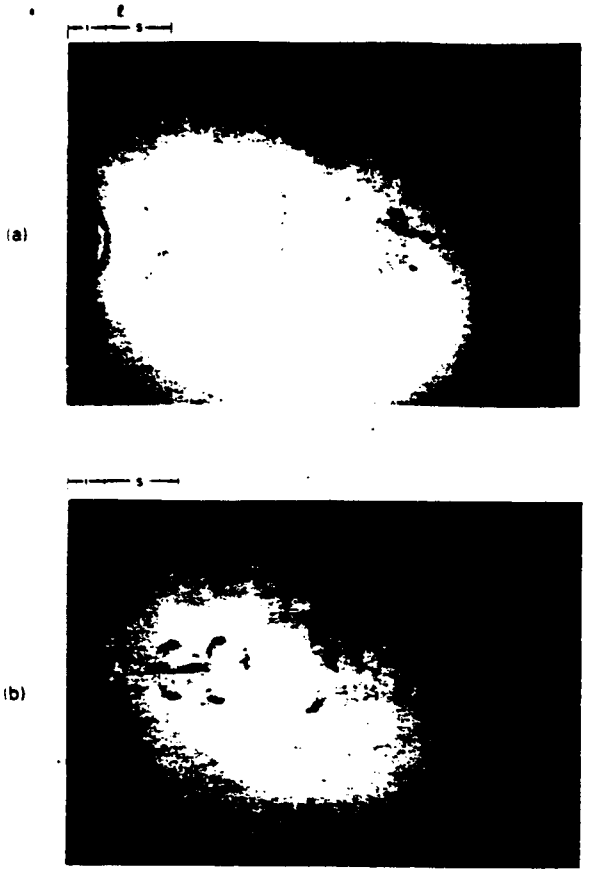

FIG. 1. Initial development region (i) and subsequent axis-switching region (s) of a forced elliptic jet in the major axis (a) and minor axis (b) planes.

These conditions are studied in Sec. III in relation to the jet-core eccentricity and azimuthal distribution of momentum thickness, and in Sec. IV in relation to jet compressibility. In Sec. V, streak-line patterns are plotted for flow regimes ranging from low subsonic to supersonic in order to demonstrate explicitly the initial deformation.

II. STABILITY ANALYSIS FOR ELLIPTIC JETS[13]

We express the velocity profile of a 3-D straight jet in an inviscid compressible fluid with incremental pressure p and density ρ as

$$\mathbf{U} = W(x,y)\hat{e}_z + \mathbf{u}, \tag{1}$$

where $W\hat{e}_z$ is the jet mean flow velocity ($W > 0$) and $\mathbf{u}$ is the fluctuating velocity associated with spatial instabilities. Application of the linearized momentum and mass-conservation equations and the assumed (z,t) dependence,

$$e^{i(\alpha z - \omega t)}, \tag{2}$$

yields

$$(\nabla^2 - \tilde{\alpha}_C^2)p + \nabla p \cdot \nabla \ln[\bar{\rho}^{1/\gamma}/\bar{p}(\omega - \alpha W)^2] = 0, \tag{3}$$

where

$$\tilde{\alpha}_C^2 = \alpha^2\{1 - [(\omega/\alpha - W)/a]^2\}, \tag{4}$$

$\bar{p}$ is the time averaged pressure (assumed to be independent of position),

$$\nabla = \hat{e}_x \frac{\partial}{\partial x} + \hat{e}_y \frac{\partial}{\partial y}, \tag{5}$$

and a is the local sound speed, which is related to the time averaged temperature $\bar{T}$ and density $\bar{\rho}$ by

$$a = a_0\sqrt{\bar{T}/\bar{T}_0} = a_0\sqrt{\bar{\rho}_0/\bar{\rho}}, \tag{6}$$

where a_0, $\bar{T}_0$, and $\bar{\rho}_0$ are the sound speed, temperature, and flow density at the origin of the coordinates, respectively. It is assumed that the temperature and the mean velocity are related according to the Busemann–Crocco law,[14]

$$T = T_0\left[T_r + (1 - T_r)\frac{W}{W_0} + \frac{\gamma - 1}{2}M_0^2\frac{W}{W_0}\left(1 - \frac{W}{W_0}\right)\right], \tag{7}$$

where $T_r = T_1/T_0$, $T_1 = T(\sqrt{x^2 + y^2} \to \infty)$, $M_0 = W_0/a_0$, and γ is the ratio of the specific heats.

For a given ω, the solution of Eq. (3) with p finite and $\to 0$ for $\sqrt{x^2 + y^2} \to \infty$, yields the corresponding eigenvalue wavenumber ($\mathrm{Re}\{\alpha\}$) and spatial growth rate ($-\mathrm{Im}\{\alpha\}$).

We assume elliptic-core jets whose mean flows $W(r,\phi)$ (r,ϕ: polar coordinates) have the symmetry properties

$$W(r,\phi + \pi) = W(r,\phi) = W(r,\pi - \phi). \tag{8}$$

The general classification of eigenmodes for this type of mean flow is discussed in Refs. 9–11. In this paper, we will consider in detail only the behavior of the eigenmodes of the $+\ +$ or ce_{2m} symmetry class, for which

$$p(r,\pi - \phi) = p(r,\phi) = p(r,\pi + \phi). \tag{9}$$

For circular jets, this class corresponds to the individual ϕ dependences $\cos 2m\phi$, $m = 0,1,2,\ldots$. In general, for jets with mean flows satisfying Eq. (8), the $+\ +$ eigenmodes may be represented as

$$p_{++}^{(2n)}(r,\phi) = \sum_{m=0}^{\infty} A_{2m}^{(2n)}(r)\cos 2m\phi, \quad n = 1,2,3,\ldots. \tag{10}$$

Simple orthogonality relations among the eigenmodes of Eq. (3) do not exist. However, we can apply the biorthogonal relations[15–18] derived in the Appendix to extract a particular eigenmode from a general $+\ +$ expansion of p.

The spatial coordinates, D and θ, are used to specify the mean flow are indicated in Fig. 2. The core region, with $W = W_0$ constant, is bounded by the ellipse shown. The Cartesian coordinates (x_e, y_e) of a point on this ellipse are

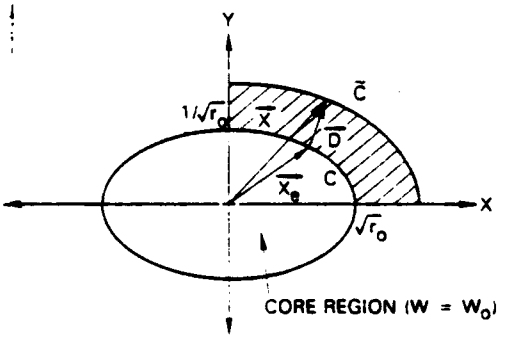

FIG. 2. Spatial coordinates used to specify the mean flow $W(D,\theta)$, as described in the text. The crosshatched region in the first quadrant, where $|\nabla W|$ is non-negligible, is the effective calculational domain for Eq. (3).

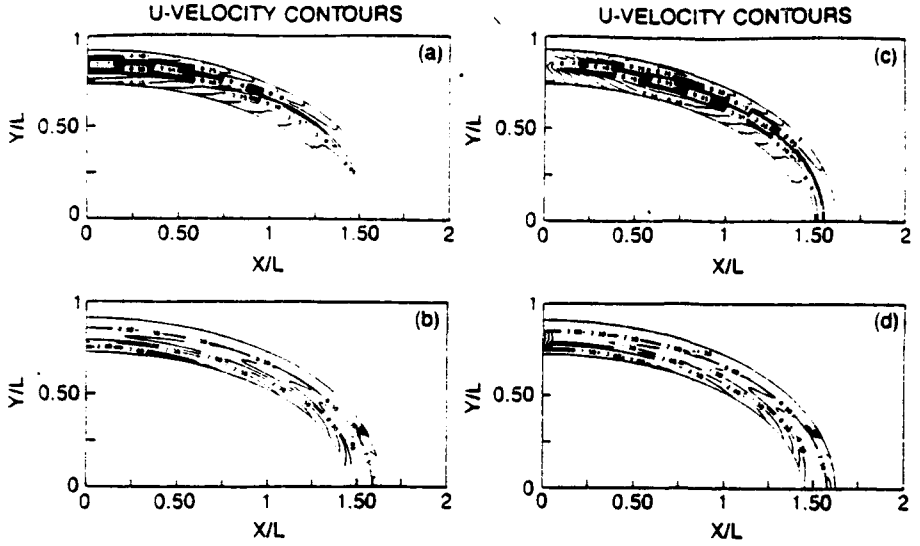

FIG. 3. Contour plots of the magnitude and phase of the eigenfunctions for the streamwise-fluctuation-velocity component u_z, for frequency $\omega = 5.4$, $A/B = 2$, and specification 0.02/0.02 for the momentum thickness variation [the first and second numbers refer to the momentum thickness along the major and minor axes, respectively; θ_0 and c_1 are found from Eq. (14)]. The magnitudes [(a) and (c)] and phases [(b) and (d)] correspond to the most unstable eigenmode of the + + and − − class, respectively. The solid and dashed lines represent positive and negative phase contours.

$$x_e = \sqrt{r_0}\cos\theta,$$
$$y_e = (1/\sqrt{r_0})\sin\theta, \tag{11}$$

where $r_0 = A/B$, with A and B being the lengths of the semimajor axis and semiminor axis, respectively; θ is the elliptic coordinate angle; and x_e and y_e are nondimensionalized by $L = \sqrt{AB}$. A given point $\mathbf{x} = (x,y)$ outside this ellipse is then specified by D, the distance from the point to the ellipse along a line perpendicular to the ellipse, and θ, the elliptic coordinate angle of the point on the ellipse intersected by this line.

By using the symmetry relations of Eq. (9), the computation region for Eq. (3) may be effectively reduced to that contained in the first quadrant (crosshatched in Fig. 2). The same reduction of the computation region holds for the other symmetry classes.[13]

Calculations were done using the mean flow

$$W(D,\theta) = \frac{1}{2}\left[1 - \tanh\left(\frac{D + D_s(\theta)}{2\Theta(\theta)}\right)\right], \tag{12}$$

where $\Theta(\theta)$ is the momentum thickness and $D_s(\theta)$ is given by

$$D_s(\theta) = \Theta(\theta)\ln[(1 - W_1)/W_1]. \tag{13}$$

In Eq. (13) W_1 is a number close to unity. All velocities, lengths, and temperature are nondimensionalized by W_0, L, and T_0, respectively. For the calculations of this paper, we have used the momentum thickness function,

$$\Theta(\theta) = \theta_0[1 + c_1 S(\theta)/S(\pi/2)], \tag{14}$$

where c_1 is a constant for controlling the azimuthal variation of momentum thickness and $S(\theta)$ is the arclength along the curve c from $(x_e(0), y_e(0))$ to $(x_e(\theta), y_e(\theta))$.

In applying finite difference techniques to the solution of Eq. (3), the crosshatched region of the x-y plane in Fig. 2 is thus transformed to a rectangular region of the θ-D plane.

III. INSTABILITY MODES FOR INCOMPRESSIBLE FLOWS

In order to assess the effects of compressibility, we first investigate the behavior of the spatial instability eigenmodes when the flow is considered to be incompressible.

In Figs. 3 and 4, contour plots are shown for magnitude $|u_z|$ and phase ϕ_z of the streamwise-velocity-fluctuation

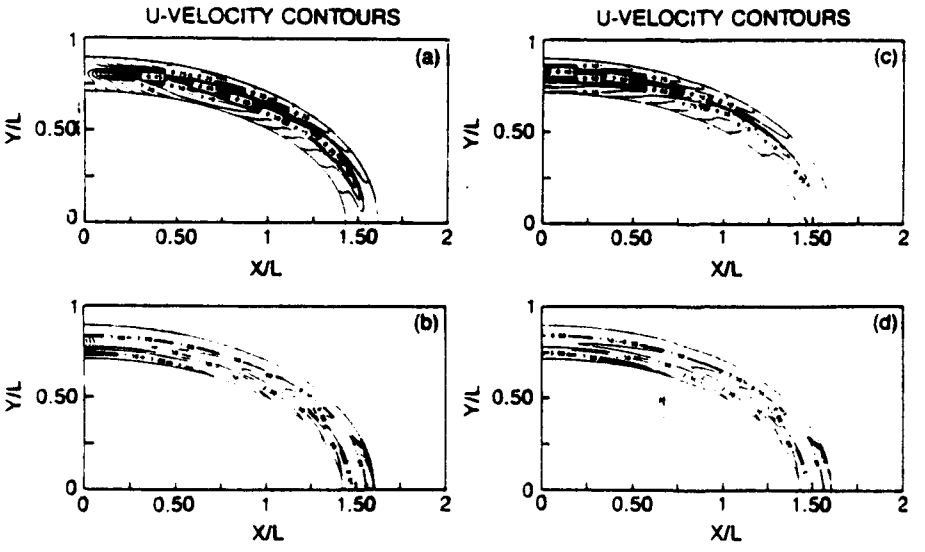

FIG. 4. Contour plots for the magnitude and phase of u_z for the same conditions as in Fig. 3. The magnitudes [(a) and (c)] and phases [(b) and (d)] correspond to the most unstable eigenmodes of the − + and + − class, respectively. Most unstable eigenmodes of various classes are implied for all subsequent figures, unless otherwise stated.

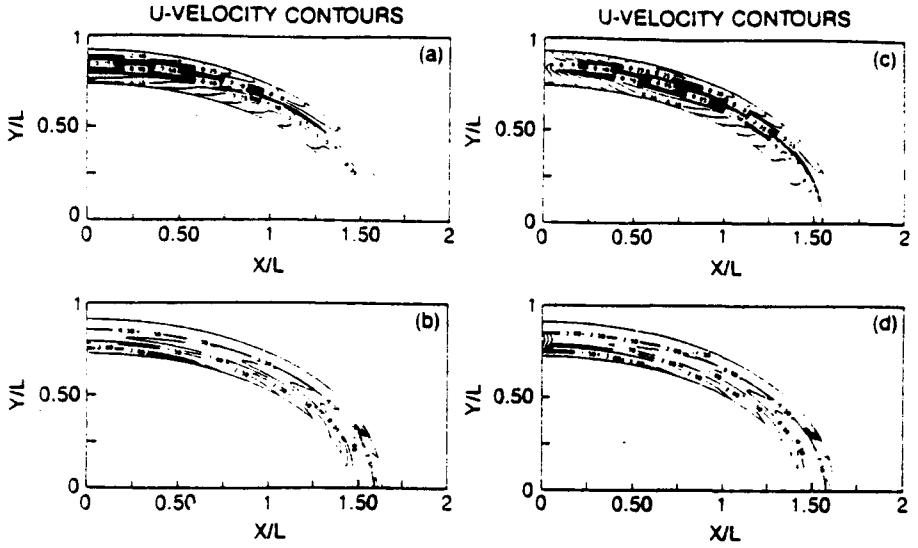

FIG. 3. Contour plots of the magnitude and phase of the eigenfunctions for the streamwise-fluctuation-velocity component u_r, for frequency $\omega = 5.4$, $A/B = 2$, and specification 0.02/0.02 for the momentum thickness variation [the first and second numbers refer to the momentum thickness along the major and minor axes, respectively; θ_1 and c_1 are found from Eq. (14)]. The magnitudes [(a) and (c)] and phases [(b) and (d)] correspond to the most unstable eigenmode of the $+\ +$ and $-\ -$ class, respectively. The solid and dashed lines represent positive and negative phase contours.

$$x_e = \sqrt{r_0}\cos\theta,$$
$$y_e = (1/\sqrt{r_0})\sin\theta, \tag{11}$$

where $r_0 = A/B$, with A and B being the lengths of the semimajor axis and semiminor axis, respectively; θ is the elliptic coordinate angle; and x_e and y_e are nondimensionalized by $L = \sqrt{AB}$. A given point $\mathbf{x} = (x,y)$ outside this ellipse is then specified by D, the distance from the point to the ellipse along a line perpendicular to the ellipse, and θ, the elliptic coordinate angle of the point on the ellipse intersected by this line.

By using the symmetry relations of Eq. (9), the computation region for Eq. (3) may be effectively reduced to that contained in the first quadrant (crosshatched in Fig. 2). The same reduction of the computation region holds for the other symmetry classes.[13]

Calculations were done using the mean flow

$$W(D,\theta) = \frac{1}{2}\left[1 - \tanh\left(\frac{D + D_s(\theta)}{2\Theta(\theta)}\right)\right], \tag{12}$$

where $\Theta(\theta)$ is the momentum thickness and $D_s(\theta)$ is given by

$$D_s(\theta) = \Theta(\theta)\ln[(1 - W_1)/W_1]. \tag{13}$$

In Eq. (13) W_1 is a number close to unity. All velocities, lengths, and temperature are nondimensionalized by W_0, L, and T_0, respectively. For the calculations of this paper, we have used the momentum thickness function,

$$\Theta(\theta) = \theta_0[1 + c_1 S(\theta)/S(\pi/2)], \tag{14}$$

where c_1 is a constant for controlling the azimuthal variation of momentum thickness and $S(\theta)$ is the arclength along the curve c from $(x_e(0), y_e(0))$ to $(x_e(\theta), y_e(\theta))$.

In applying finite difference techniques to the solution of Eq. (3), the crosshatched region of the x-y plane in Fig. 2 is thus transformed to a rectangular region of the θ-D plane.

III. INSTABILITY MODES FOR INCOMPRESSIBLE FLOWS

In order to assess the effects of compressibility, we first investigate the behavior of the spatial instability eigenmodes when the flow is considered to be incompressible.

In Figs. 3 and 4, contour plots are shown for magnitude $|u_r|$ and phase ϕ_r of the streamwise-velocity-fluctuation

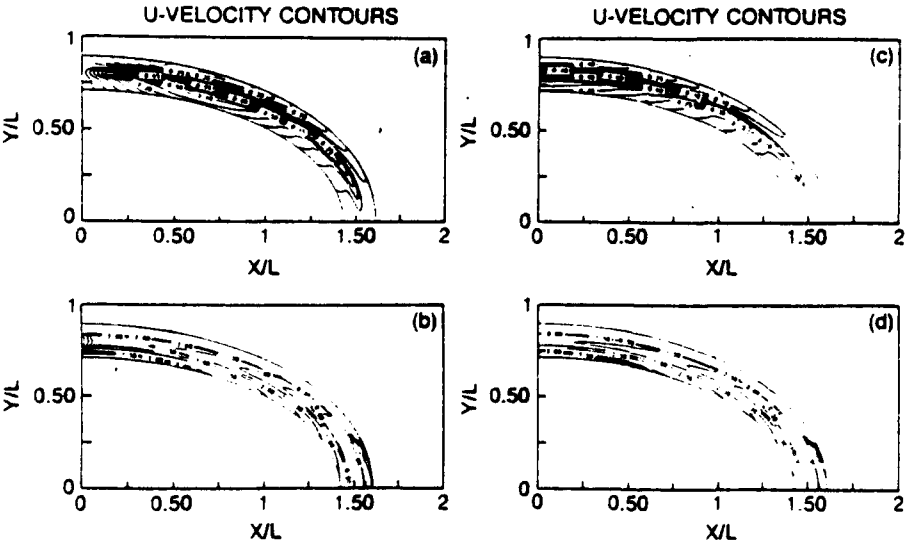

FIG. 4. Contour plots for the magnitude and phase of u_r for the same conditions as in Fig. 3. The magnitudes [(a) and (c)] and phases [(b) and (d)] correspond to the most unstable eigenmodes of the $-\ +$ and $+\ -$ class, respectively. Most unstable eigenmodes of various classes are implied for all subsequent figures, unless otherwise stated.

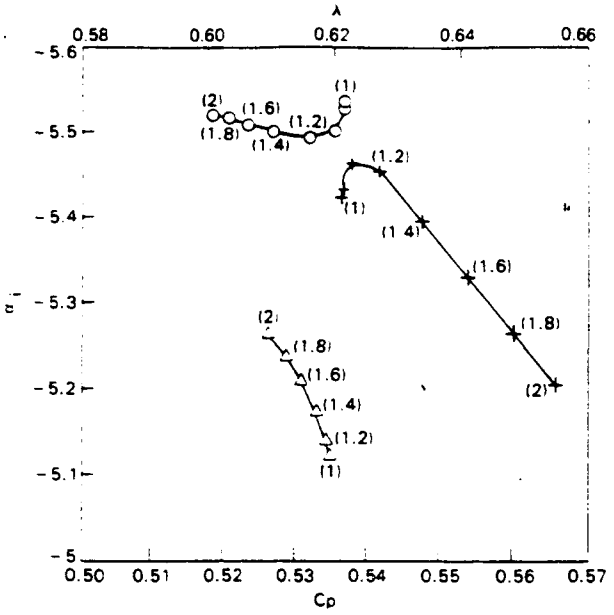

FIG. 6. Core eccentricity dependence of the eigenvalues which track from those of the $m = 0$ (circle), 2 (plus), and 4 (triangle) modes of a circular-core jet for $\omega = 5.4$ and 0.02/0.02, in the negative-of-the-growth rate (α_i), phase speed (C_p), and wavelength (λ) plane. The numbers in parentheses are for A/B.

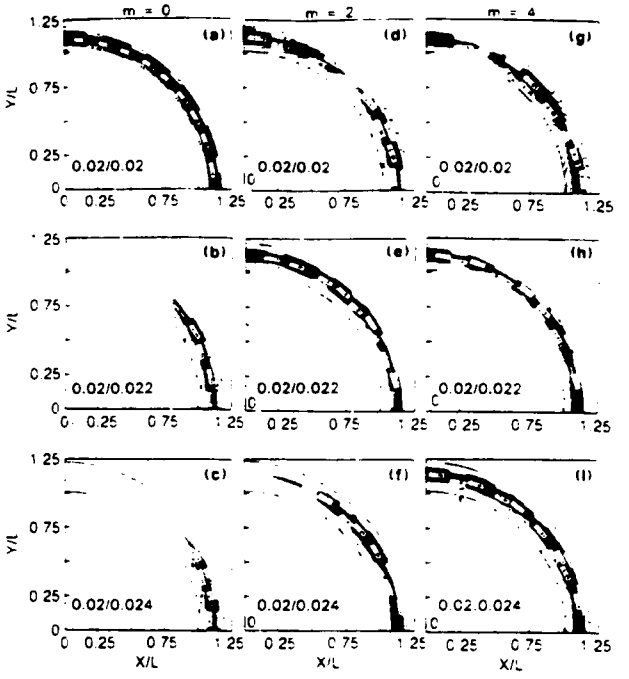

FIG. 7. Contour plots of $|u_z|$ for the evolution of the $m = 0$ (a)–(c), $m = 2$ (d)–(f), and $m = 4$ (g)–(i) modes of a circular-core jet ($A/B = 1$) for $\omega = 5.4$ and variation of momentum thickness specified by 0.02/0.02, 0.02/0.022, and 0.02/0.024 from top to bottom.

lar-jet mode, an analogy to the situation for the eigenfunctions, has phase speeds which are intermediate with respect to the phase-speed extremes of the $+ +0$ and $+ +2$ modes. The spatial growth rates for this mode are comparable to those of the other two modes. The essential behavior of the three eigenmodes can be summarized by three conditions: (1) proper localizations of eigenfunctions without excessive overlapping; (2) sufficiently large differences in phase speeds; and (3) comparable spatial growth rates. Fulfillment of these three conditions by the eigenmodes may be associated with the deformation in the initial state of the axis switching of elliptic-core jets. This point will be demonstrated in Sec. V.

B. Effects of azimuthal distribution of momentum thickness

The Kelvin–Helmholtz instability is associated with a vorticity maximum in the velocity profile. In a 2-D shear layer, the value of the maximum vorticity is a constant in the transverse direction. However, this is not true in a 3-D flow. The azimuthal variation of the momentum thickness will certainly influence the characteristics of the instability modes and can be used as an extra flow control property for manipulating the instabilty waves.

We now investigate the effect of azimuthal variation of the momentum thickness on the eigenmode behaviors. For $A/B = 1$ the contour plots of Fig. 7 show that, for all three modes, the location of maximum streamwise velocity fluctuations coincides with the location of the minimum thickness. In contrast to the situation for elliptic jets, there is no indication of polarization of eigenmode activities among the three modes. Furthermore, the associated variations of the eigenvalues in Fig. 8 show that the phase-speed differences are greatly reduced and the higher modes have significant reductions in the spatial growth rates. Therefore, the three conditions are not satisfied for this case, and the possibility of simulating the elliptic-jet behavior (the effects of core eccentricity) using circular-core jets with nonuniform momentum thickness distributions is remote.

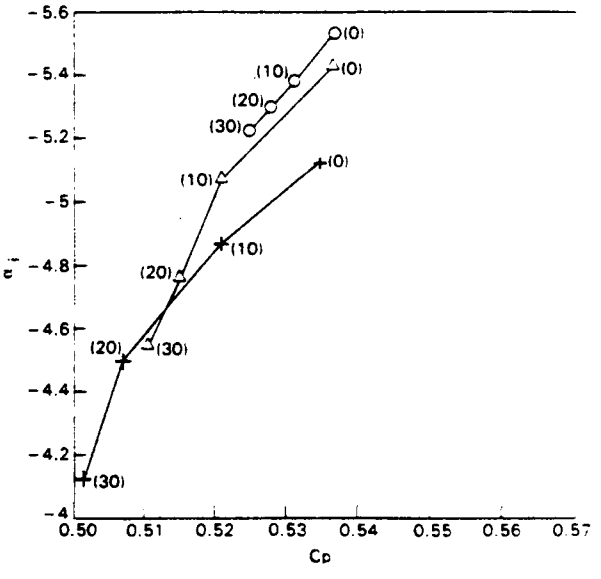

FIG. 8. The evolution (with changes in the momentum thickness azimuthal dependence) of the $m = 0$ (circle), 2 (triangle), and 4 (plus) modes of a circular-core jet ($A/B = 1$) for $\omega = 5.4$, in the negative-of-the-growth rate (α_i), phase-speed (C_p) plane. The numbers in parentheses are the values for the percentage change in momentum thickness specification (10% change = 0.02/0.022, etc.).

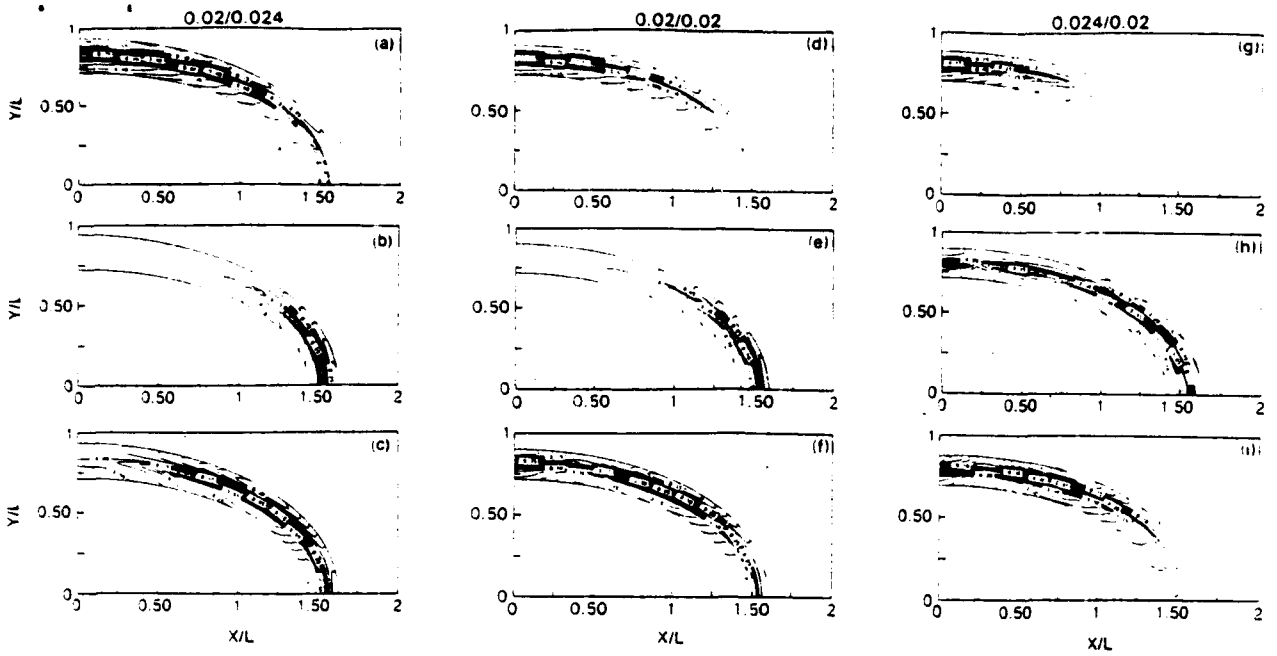

FIG. 9. Contour plots of $|u_z|$ for the $+ +0$, $+ +2$, and $+ +4$ eigenmodes (from top to bottom of the figure) for 0.02/0.024 (a)–(c), 0.02/0.02 (d)–(f), 0.024/0.02 (g)–(i), and $\omega = 5.4$, $A/B = 2$.

The effects of azimuthal variation of momentum thickness on eigenfunctions for $A/B = 2$ are given in Fig. 9. The contour plots for $|u_z|$ are displayed for momentum thicknesses (0.02, 0.024) along the (major, minor) axes (a). It is seen that the spatial concentrations of the eigenfunctions are shifted toward the major axis where the momentum thickness is minimal. For the reverse situation, with momentum thicknesses (0.024, 0.02) along the (major, minor) axes (c), it is found that the eigenfunction concentrations are shifted toward the minor axis [compare with the uniform momentum thickness case (0.02, 0.02) (b)]. Thus the effects of momentum thickness can be used to modify the eigenfunction properties associated with the core eccentricity. The localization characteristics (condition 1) among the eigenmodes still exist for these momentum thickness variations (maximum variation 20%). However, a further increase in the variation can destroy the validity of condition 1, with all of the significant eigenfunction activities becoming concentrated near the region of minimum momentum thickness. Note also that the localizations of eigenfunctions with momentum thicknesses (0.02/0.024) show polarizations more distinct than those for the reverse situation with the momentum thicknesses (0.024/0.02). Therefore, increasing momentum thickness along the major axis while keeping the momentum thickness along the minor axis constant appears to lead to an invalidation of condition 1. A similar situation is found in the behaviors of corresponding eigenvalues, which will be discussed in the following.

In Fig. 10, we show the variation of the eigenvalues of the modes for $A/B = 2$ when (major, minor) axis variations of the momentum thickness are changed from (0.02, 0.024) to (0.024, 0.02) in 5% increments at three different frequencies (below, at, and above the frequency of maximum amplification). The effects of varying the momentum thickness are clearly different for different frequencies. However, it is seen that for all frequencies considered, the eigenvalues for

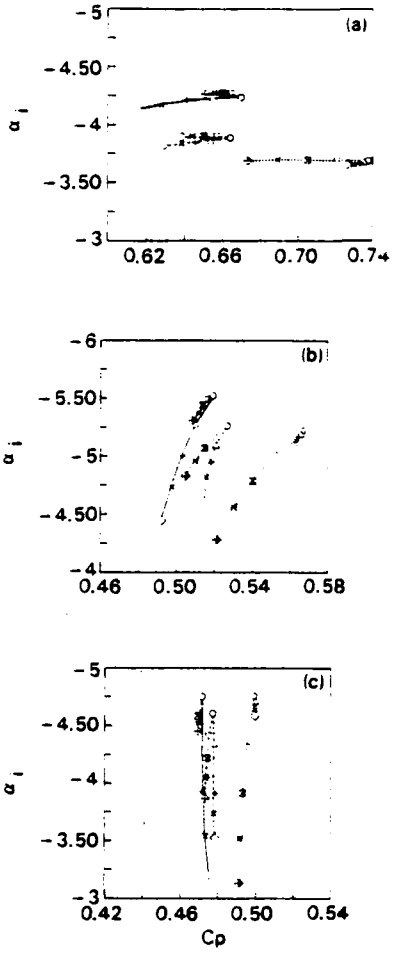

FIG. 10. Eigenvalues for the $+ +0$ (solid line), $+ +2$ (dotted line), and $+ +4$ (dashed line) eigenmodes of a jet with $A/B = 2$ in the negative-of-the-growth rate (α_i), phase-speed (C_p) plane, for $\omega = 3.6$ (a), 5.4 (b), and 7.2 (c). The variations of momentum thicknesses are 0.02/0.024 (◇), 0.02/0.023 (×), 0.02/0.022 (+), 0.02/0.021 (△), 0.02/0.02 (○), 0.021/0.02 (▽), 0.022/0.02 (⊠), 0.023/0.02 (*), 0.024/0.02 (◆).

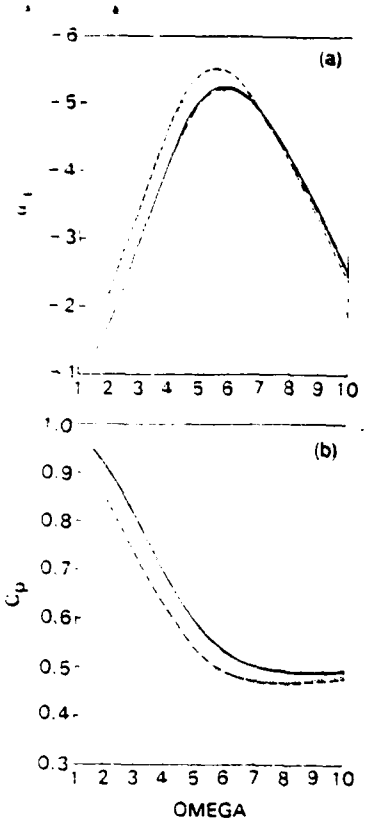

FIG. 11. The negative-of-the-growth-rate (α_i) and phase speed (C_p) versus frequency ω for eigenmodes corresponding to $A/B = 2$; + +0, 0.02/0.02 (dashed line); + +0, 0.02/0.021 (dotted line); + +2, 0.02/0.02 (solid line); and + +2, 0.02/0.021 (dash–dot line).

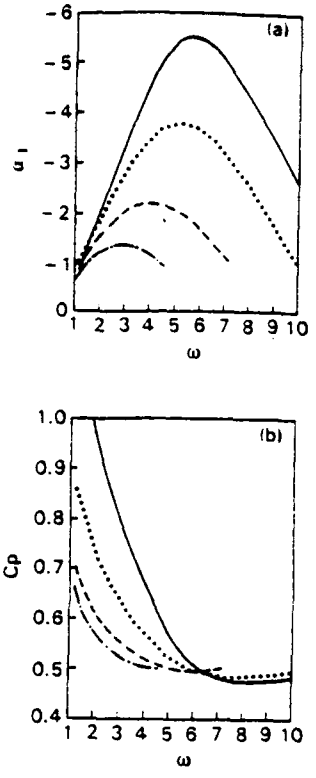

FIG. 12. The negative-of-the-growth-rate (α_i) (a) and phase speed (C_p) (b) versus frequency ω for eigenmodes corresponding to $A/B = 1$; + +0, 0.02/0.02; and Mach number M_0, 0 (solid line), 1 (dotted line), 1.5 (dashed line), and 1.75 (dash–dot line).

the + +0(2) mode are most sensitive to variations of momentum thickness in the neighborhood of either axis. At the most amplified frequency (b), it is found that increasing the momentum thickness along the minor axis and keeping the momentum thickness along the major axis constant increases the phase-speed difference between the + +0 and + +2 modes, whereas the reverse situation for the azimuthal momentum thickness along the major axis constant increases the phase-speed difference between the + +0 and + +2 modes, whereas the reverse situation for the azimuthal momentum thickness distribution decreases the phase-speed difference. These variations in azimuthal momentum thickness distribution increase the differences in growth rates for the eigenmodes, however. Increasing the momentum thickness along the minor axis creates less change in the difference in the spatial growth rates among the eigenmodes than the reverse case [e.g., comparison between the cases (0.02/0.024) and (0.024/0.02) shows that the difference in the spatial growth rates for the first case is about half of that for the second case]. Thus increasing the momentum thickness along the major axis appears to invalidate conditions 2 and 3 for the deformation. In Fig. 11, the eigenvalue variations are given for a continuum of ω values for momentum thicknesses of (0.02, 0.02), and (0.02, 0.021) along the (major, minor) axes. It is apparent from Fig. 11 that selection of frequency (e.g., choice of 5 or 6 for ω) does not alter the above findings for the eigenvalue behaviors of the two modes, + +0 and + +2 (e.g., the phase-speed difference between two modes shown in Fig. 6 is very nearly independent of frequency).

IV. STABILITY MODES IN COMPRESSIBLE FLOWS

In studying the effects of compressibility, the value γ for the ratio of specific heats is assumed to be 1.4, and we only consider the homogeneous temperature case, with $T_r = 1$ in Eq. (7), and (uniform) momentum thickness 0.02. In Fig. 12, the spatial growth rates ($-\alpha_i$) and phase speeds C_p are plotted as functions of ω for the $m = 0$ mode of a circular jet for Mach numbers 0, 1.0, 1.5, and 1.75. Michalke[14] investigated the effect of Mach number on the instability of circular jets. It is not possible to quantitatively compare our results with this jet since the jet parameter (the ratio of jet radius to the momentum thickness) and the Mach numbers used in the two calculations are different. However, the effects of Mach number on the qualitative behaviors of the spatial growth rates are similar. The frequencies for the most amplified modes for $M_0 = 1$, 1.5, and 1.75 are approximately equal to 5.0, 3.8, and 2.9, respectively. In Fig. 13, contour plots of $|u_z|$ are given for elliptic-core ($A/B = 2$) modes + +0, 2, and 4, with $M_0 = 1$ (a)–(c), 1.5 (d)–(f), and 1.75 (g)–(i) for $\omega = 5.0$, 3.8, and 2.9, respectively. It is interesting to see that, with increasing eccentricity, the eigenfunctions tracking from the $m = 0(2)$ circular-core modes become more localized toward the major (minor) axis. These trends are just the opposite of those for incompressible flow [see Figs. 5(a)–5(f) and Figs. 9(d) and 9(e)]. A simi-

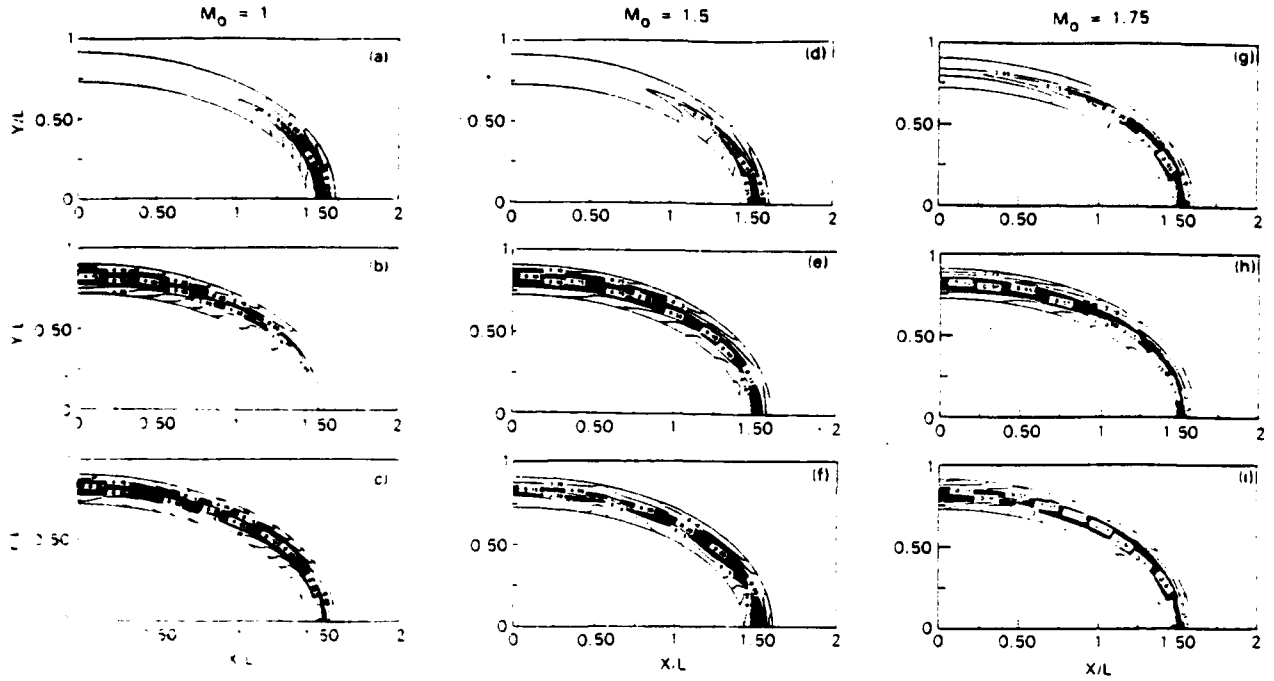

FIG. 13. Contour plots of u, for $- +0$, $- +2$, $- +4$ eigenmodes (from top to bottom in the figure) for flow Mach number $M_0 = 1$ (a)–(c), 1.5(d)–(f), and 1.75(g)–(i), and $A/B = 2$, 0.02/0.02. The frequency corresponding to maximum amplification is used for each flow Mach number.

lar switch in the behavior of the corresponding eigenvalues is seen in Fig. 14. The switching in the behavior of the eigenmodes occurs approximately at Mach number 0.45 as shown in Fig. 15. It is clearly shown in Fig. 13 that the eigenfunction localizations decrease for all three modes as flow Mach number increases. This tendency to invalidate condition 1 is combined with one to invalidate condition 3 (due to the dominant growth rate of the $+ +4$ mode as shown in Fig. 14). These result (see Sec. V) in a gradual decrease of rollup location difference in streak-line patterns as flow Mach number increases.

V. STREAK-LINE PATTERNS

Since the eigenfunctions and the corresponding eigenvalues are known, it is possible to calculate the streak-line patterns issued from all azimuthal locations in order to demonstrate the deformation seen in Fig. 1. However, it would require enormous computing efforts to accomplish this. Therefore, we do the more manageable calculation of streak-line patterns emanating from the minor and major axis planes. Another simplification in the calculation is due to the assumption that the in-phase forcing jet selects a linear combination of fluctuation-of-velocity eigenmodes of the $+ +$ class. The coefficients of the eigenmodes may be obtained from the biorthogonal relations given in the Appendix. Michalke[19] calculated the streak-line patterns for a plane shear layer with a tanh velocity profile, and found the tendency of the streak lines to roll up. Monkewitz[20] calculated the vorticity contours at the locations where the vortex merging occurred by taking subharmonic resonance into consideration.

In Figs. 16 and 17, we give the results of streak-line calculations with time steps equal to a quarter of the period, based on superpositions of the previously discussed $- +$ modes of an elliptic jet. The projections of the streak lines are given in the minor and major axes, respectively. The parameter values used were $A/B = 2$, $\omega = 5.4$, and $M_0 = 0$. Using Eqs. (1) and (2), we followed the procedure of Michalke[19] and set the maximum u-component magnitude equal to 0.0005 at $z = 0$. It is interesting to see how the difference in modal phase speeds is manifested in the resulting streak-line patterns.

The location of a particle in the minor axis plane is governed by the equations

$$\frac{dy}{dt} = \hat{e}_y \cdot \mathbf{U} + \text{c.c.}, \tag{18a}$$

$$\frac{dx}{dt} = \hat{e}_x \cdot \mathbf{U} + \text{c.c.}, \tag{18b}$$

where c.c. denotes complex conjugate and the right-hand sides are the y and z components of the total velocities. Similar equations are obtained for the x and z coordinates of the particle position vector. The integration of the particle trajectory equations was done using a fourth-order Runge–Kutta method, with the calculational domain limited in the z direction by the requirement that the maximum of the disturbance not exceed unity. For discussion of the extent of validity of the linear stability theory for streak-line calculations, see Refs. 19 and 21.

It is clear from Figs. 16 and 17 that the difference in phase speeds is reflected in the difference of the rollup locations, with the rollup location in the semimajor plane being further downstream from that in the semiminor plane. The rollup locations in the semiminor and major planes are at approximately twice[22] the wavelength of the dominant modes [the dominant modes are shown in Figs. 9(d) and 9(e), respectively]. The difference in the rollup locations persists in the case of $M_0 = 1$, as can be seen in Figs. 18(a) and 18(b). The delays in the rollup locations relative to

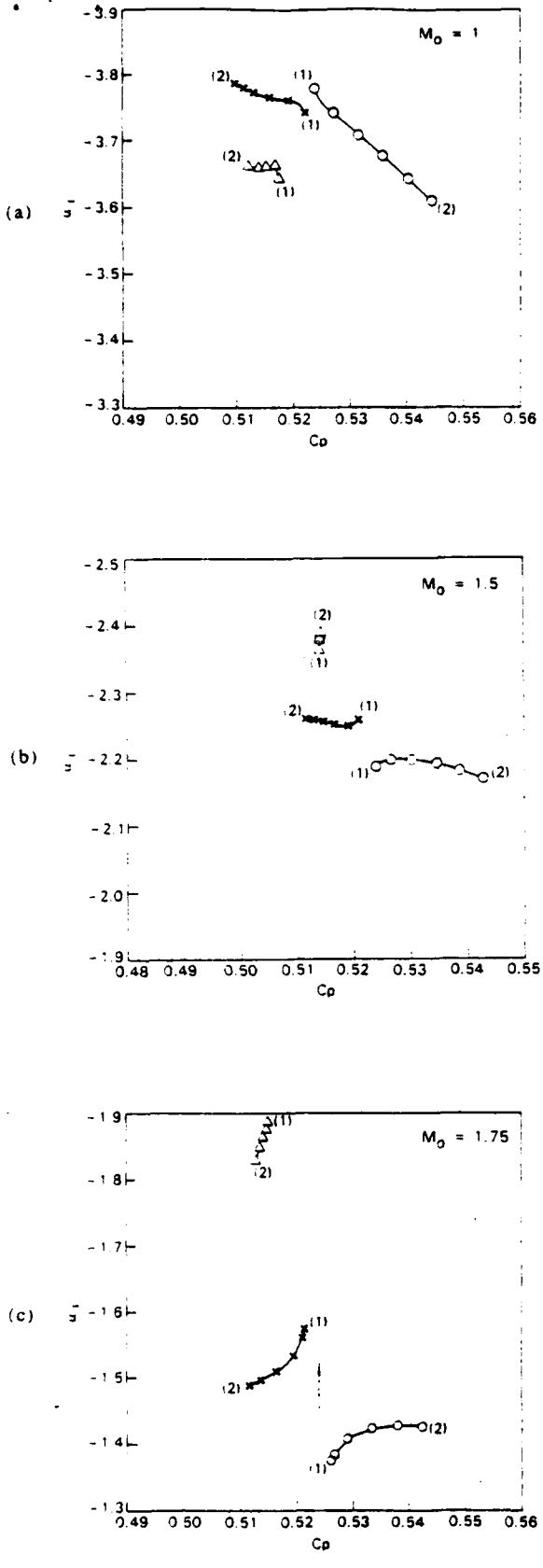

FIG. 14. Core eccentricity dependence of the eigenvalues which track from those of the $m = 0$ (circle), 2 (cross), and 4 (triangle) modes of a circular-core jet with 0.02/0.02, for Mach number $M_0 = 1$ (a), 1.5 (b), 1.75 (c), in the negative-of-the-growth rate (α_i), phase-speed (C_p) plane. The numbers in parentheses are the values of A/B. The frequency corresponding to maximum amplification is used for each flow Mach number.

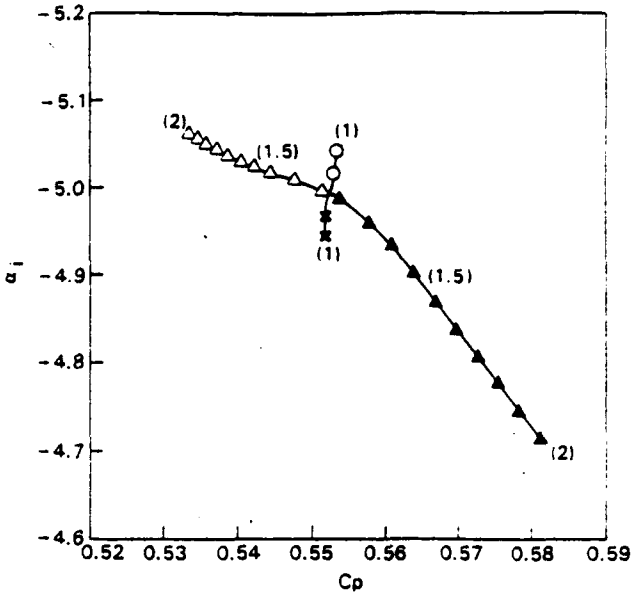

FIG. 15. Core eccentricity dependence of the eigenvalues which track from those of the $m = 0$ (circle) and 2 (cross) modes of a circular-core jet with 0.02/0.02 for Mach number $M_0 = 0.45$, in the negative-of-the-growth rate (α_i), phase-speed (C_p) plane. The numbers in parentheses are the values of A/B. The triangles indicate that the evolution tracks intersect and are thus indistinguishable with respect to their initial (1) points.

those in Figs. 16 and 17 are a result of the suppression of the growth rates due to the compressibility of the flow. The streak-line patterns for $M = 1.75$ are shown in Figs. 18(c) and 18(d). As was discussed in Sec. IV, the difficulties in satisfying conditions 1 and 3, associated with the gradual loss of eigenfunction concentrations and of comparable amplification rates among the eigenmodes (due to the domination of $+ + 4$ mode growth rate), with increasing Mach number, result in the progressive decrease of the rollup location difference as seen in Figs. 16–18.

VI. CONCLUSIONS

An attempt has been made to identify the underlying mechanisms for the deformation of coherent structures in the initial stage of axis switching of elliptic-core jets. The generalized shooting method[13] was applied to the spatial instability analysis. The calculational results showed that increasing core eccentricity gives rise to three distinctive features of groups of instability modes: (1) proper localization without excessive overlapping; (2) sufficiently large differences in phase speeds; and (3) comparable amplification rates. These features were then identified as mechanisms for the deformation of coherent structures by means of streak-line calculations. We thus consider them as conditions on the instability modes of elliptic-core jets, which are generally required if deformation of coherent structures is to occur.

The qualitative behaviors of elliptic-core jets in relation to these three conditions were studied with respect to independent and joint variations of core eccentricity, azimuthal distribution of momentum thickness, and compressibility. The possibility of simulating elliptic-core jet behavior with circular-core jets having nonuniform momentum thickness was shown to be remote. It was found that increasing the

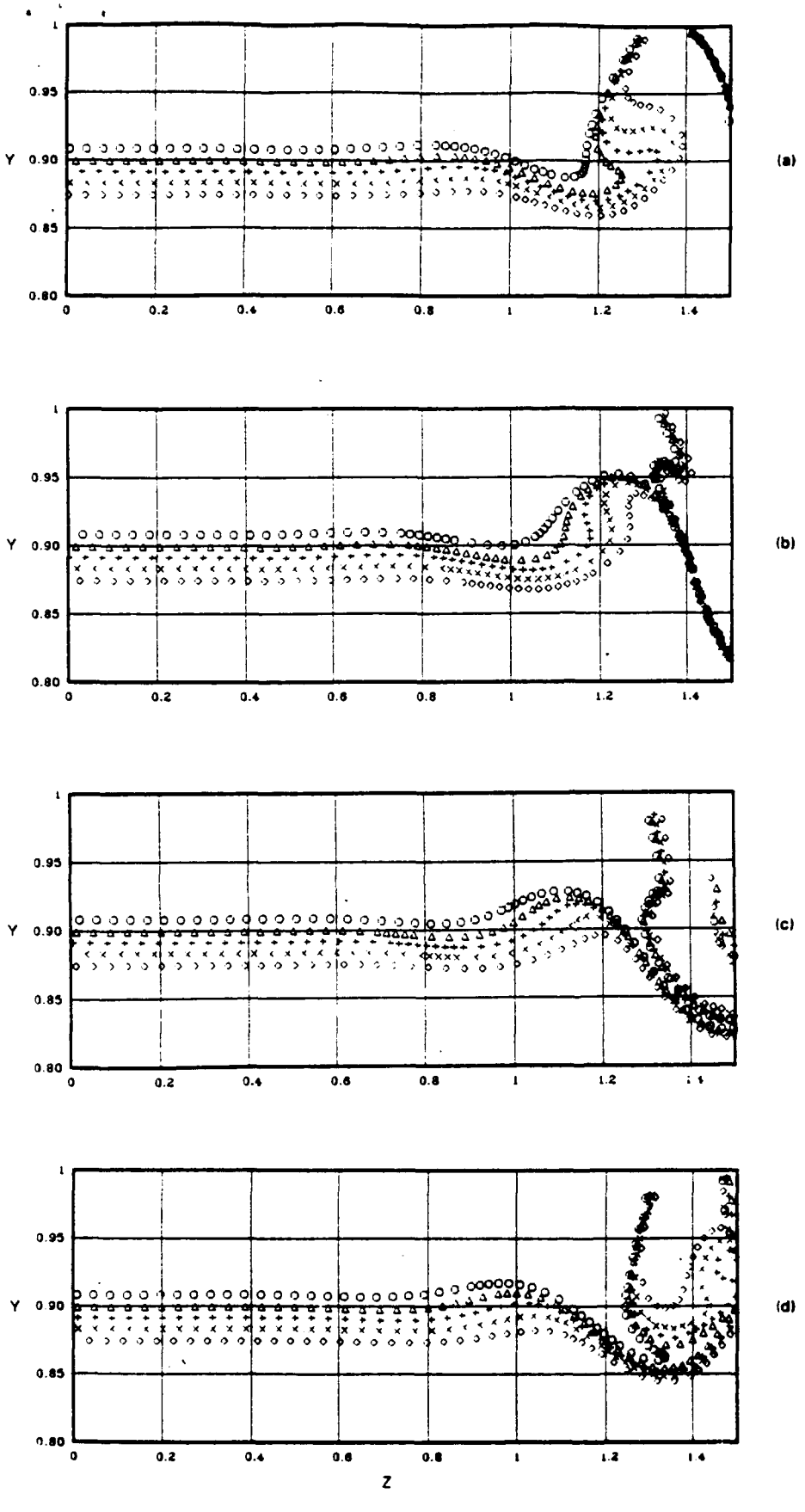

FIG. 16. Streak-line patterns in the minor axis plane of an elliptic-core jet with $A/B = 2$, 0.02/0.02, for $\omega = 5.4$ and Mach number $M_n = 0$.

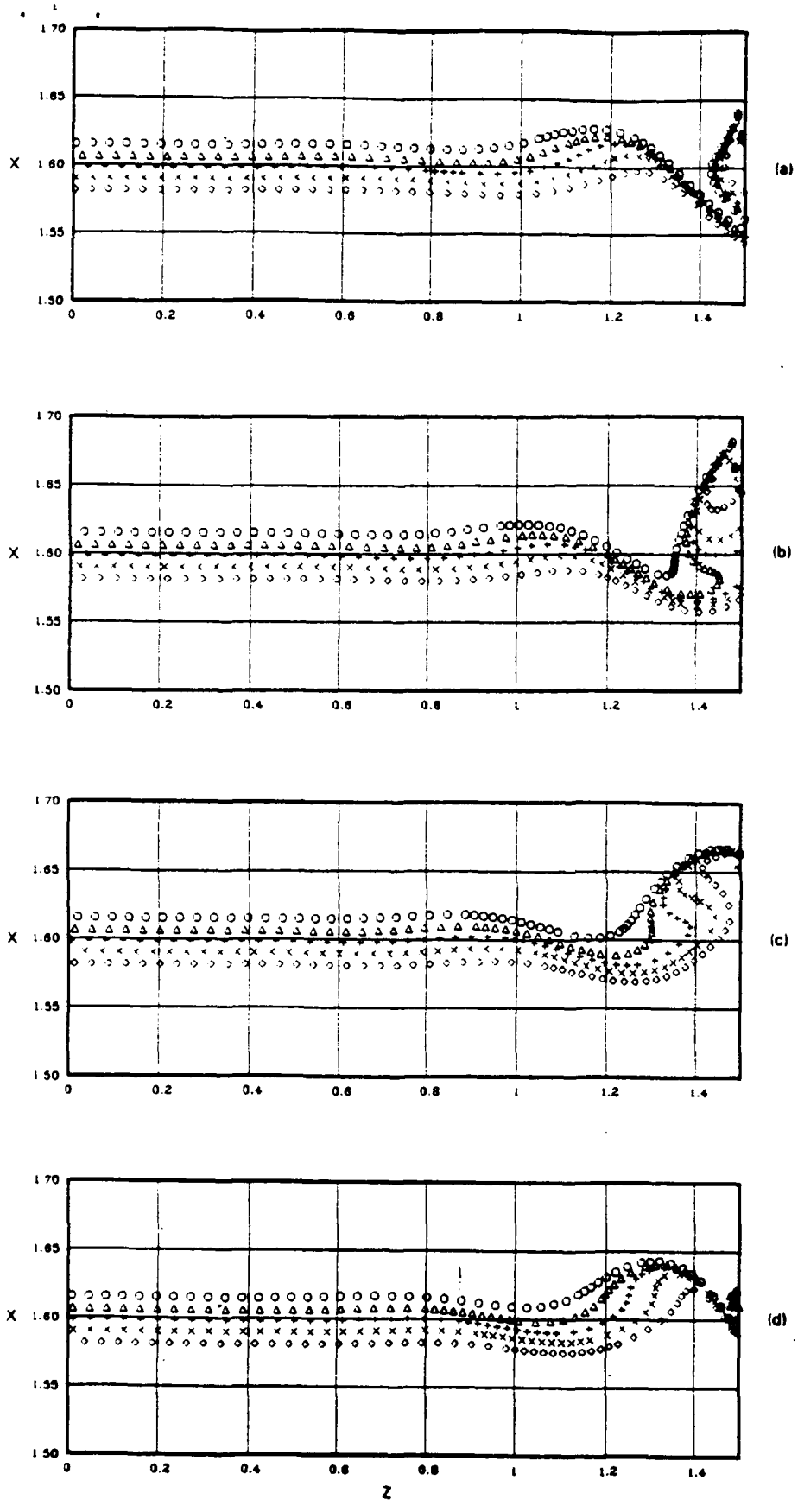

FIG. 17. Streak-line patterns in the major axis of an elliptic core with $A/B = 2$, 0.02/0.02, for $\omega = 5.4$ and Mach number $M_0 = 0$.

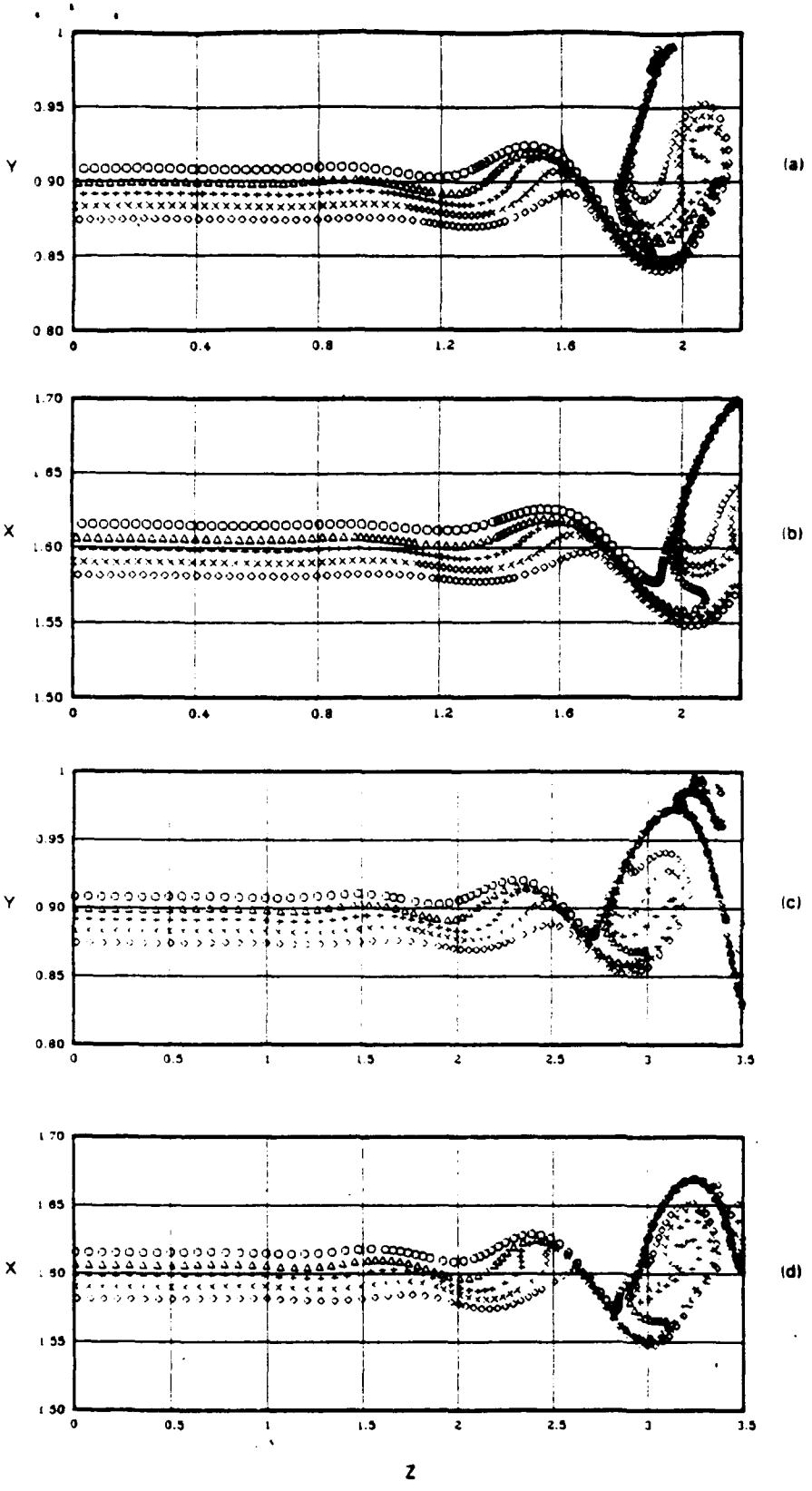

FIG. 18. Streak-line patterns in the minor axis plane for $M_0 = 1$ (a), $M_0 = 1.75$ (c), and in the major axis plane for $M_0 = 1$ (b) and 1.75 (d), of an elliptic-core jet with $A/B = 2.0/0.2/0.02$.

momentum thickness near the major axis while keeping the momentum thickness near the minor axis the same tended to invalidate the above-mentioned conditions. The possibility of realization of nonaxis switching elliptic-core jets is now under experimental investigation using the findings in this paper. Finally, it was shown that the effect of the compressibility is to deteriorate the mechanisms for the vortex deformation. Without the presence of the shock structures, our analysis showed that the deformation will not occur above the flow Mach number 1.75. Therefore we estimate 1.75 as

the upper limit of the flow Mach number for the axis switching with the eigenmodes in the + + symmetry class.

ACKNOWLEDGMENTS

We wish to thank Dr. R. L. Derr and Dr. K. C. Schadow for the encouragement given us during the course of this work; Dr. E. Gutmark for helpful discussions; and Dr. N. N. Mansour for providing access to the NAS Computer Facility, NASA Ames Research Center, Moffett Field, California.

One of us (CMH) is supported by the Air Force Office of Scientific Research Contract No. F49620-85-C-0080. One of us (AT) also wishes to thank the American Society for Engineering Education for sponsoring his summer appointments (1985–1987) at the Naval Weapons Center.

APPENDIX: BIORTHOGONAL EXPANSIONS FOR SPATIAL INSTABILITY EIGENMODES OF EQ. (3)[15–18]

For the nth eigenmode, the eigenvalue α_n, Eq. (3) may be written in the equivalent 3×3 matrix form:

$$L(\omega)|p^n\rangle = \alpha_n W(1-M^2)|p^n\rangle, \tag{A1}$$

where $|p^n\rangle$ is a column vector whose components, p_1^n, p_2^n, and p_3^n, satisfy the boundary conditions, $p_i^n \to 0$ for $\sqrt{x^2+y^2}\to\infty$; M is the local Mach number defined as $M = W(\mathbf{x})/a(\mathbf{x})$; and $L(\omega)$ is the matrix operator,

$$\begin{bmatrix} 0 & 0 & W(1-M^2) \\ 0 & \omega(1-M^2) & 2(1-M^2)\nabla W\cdot\nabla \\ W\nabla^2 + (\omega^2/a)M - (W/\bar\rho)\nabla\bar\rho\cdot\nabla & -W & -2\omega M^2 \end{bmatrix}, \tag{A2}$$

which is independent of α_n. It follows from Eqs. (A1) and (A2) that

$$p_3^n = \alpha p_1^n, \tag{A3}$$

$$\omega p_2^n + 2W\nabla W\cdot\nabla p_3^n = \alpha W p_2^n, \tag{A4}$$

and

$$\left(W\nabla^2 + \frac{\omega^2}{a}M - \frac{W}{\bar\rho}\nabla\bar\rho\cdot\nabla\right)p_1^n - Wp_2^n - 2M^2 p_3^n = \alpha W(1-M^2)\,p_3^n. \tag{A5}$$

Elimination of p_2^n and p_3^n from Eqs. (A3)–(A5) then yields Eq. (3) for p_1^n.

The adjoint form of Eq. (A1) is

$$L^+(\omega)|\tilde p^m\rangle = \alpha_m W(1-M^2)|\tilde p^m\rangle, \tag{A6}$$

where $|\tilde p^m\rangle$ is the adjoint column vector whose components, $\tilde p_1^m$, $\tilde p_2^m$, and $\tilde p_3^m$, satisfy the boundary conditions, $\tilde p_i^m \to 0$ for $\sqrt{x^2+y^2}\to\infty$; and $L^+(\omega)$ is the adjoint matrix operator,

$$L^+(\omega) = \begin{bmatrix} 0 & 0 & \nabla^2 W + (\omega^2/a)M + \nabla[(W/\bar\rho)\nabla\bar\rho] \\ 0 & \omega(1-M^2) & -W \\ W(1-M^2) & -\nabla 2(1-M^2)\nabla W & -2\omega M^2 \end{bmatrix}. \tag{A7}$$

It is easily verified that the lhs of the equation,

$$\langle\tilde p^m|L(\omega)|p^n\rangle - \langle p^n|L^+(\omega)|\tilde p^m\rangle = (\alpha_n - \alpha_m)\langle p^n|W(1-M^2)|\tilde p^m\rangle, \tag{A8}$$

vanishes, where $\langle p^n|$ is the row vector transpose of $|p^n\rangle$, and

$$\langle\tilde p^m|L(\omega)|p^n\rangle = \sum_{i,j=1}^{3}\int_{-\infty}^{\infty}dx\int_{-\infty}^{\infty}dy\,\tilde p_i^m L_{ij}(\omega)p_j^n, \text{ etc.} \tag{A9}$$

This follows from the fact that the area integral of the lhs of Eq. (A8) may be converted into a (vanishing) integral over the infinite boundary of the region of integration. Thus, for $\alpha_n \neq \alpha_m$, the second factor on the rhs of Eq. (A8) vanishes. Using Eqs. (A3)–(A7), this result may be expressed as

$$\int_{-\infty}^{\infty}dx\int_{-\infty}^{\infty}dy\,p_1^n\tilde L(W\tilde p_3^m) = 0, \tag{A10}$$

where

$$\tilde L = \frac{-\omega}{\omega-\alpha_n W}\nabla\left(\frac{\nabla W}{\omega-\alpha_m W}\right) + \left(\frac{\omega M}{a} + \frac{\alpha_n+\alpha_m}{2}(1-M^2) - \frac{\alpha_n\omega|\nabla W|^2}{(\omega-\alpha_m W)(\omega-\alpha_n W)^2}\right). \tag{A11}$$

If we now assume the general expansion

$$p(\mathbf{x}) = \sum_{n=1}^{\infty} a_n p_1^n(\mathbf{x}), \tag{A12}$$

we may use Eq. (A10) to determine the expansion coefficients a_m as

$$a_m = \frac{\int_{-\infty}^{\infty}dx\int_{-\infty}^{\infty}dy\,\tilde L(W\tilde p_3^m)p(\mathbf{x})}{\int_{-\infty}^{\infty}dx\int_{-\infty}^{\infty}dy\,\tilde L(W\tilde p_3^m)p_1^m(\mathbf{x})}. \tag{A13}$$

[1] G. L. Brown and A. Roshko, in *Turbulent Shear Flow*, AGARD-CP-93 (NATO, Brussels, 1971), p. 23.1.
[2] C. M. Ho and L. S. Huang, J. Fluid Mech. **119**, 443 (1982).
[3] D. Oster and I. Wygnanski, J. Fluid Mech. **123**, 91 (1982).

[4]M. Lee and W. C. Reynolds, Bull. Am. Phys. Soc. **28**, 1362 (1983).
[5]C. M. Ho and E. Gutmark, J. Fluid Mech. **179**, 383 (1987).
[6]K. C. Schadow, E. Gutmark, D. M. Parr, and K. J. Wilson, in *Proceedings of the 23rd JANNAF Combustion Meeting*, CPIA Pub. No. 457 (Chemical Propulsion Information Agency, Baltimore, MD, 1986), Vol. I, p. 241.
[7]M. Gaster, E. Kit, and I. Wygnanski, J. Fluid Mech. **150**, 23 (1985).
[8]D. G. Crighton, J. Fluid Mech. **59**, 665 (1973).
[9]S. Koshigoe and A. Tubis, Phys. Fluids **29**, 3982 (1986).
[10]P. J. Morris, to appear in AIAA J.
[11]P. G. Drazin and W. H. Reid, *Hydrodynamic Stability* (Cambridge U.P., Cambridge, 1981), pp. 207–211.
[12]M. R. Dhanak and B. DeBernardinis, J. Fluid Mech. **109**, 189 (1981).
[13]S. Koshigoe and A. Tubis, Phys. Fluids **30**, 1715 (1987).
[14]A. Michalke, NASA Tech. Memo 75109, 1977.
[15]P. M. Morse and H. Feshbach, *Methods of Theoretical Physics* (McGraw-Hill, New York, 1953).
[16]P. G. Drazin and W. H. Reid, in Ref. 14, p. 158.
[17]R. C. DiPrima and G. J. Habetler, Arch. Ration. Mech. Anal. **218**, 34 (1969).
[18]H. Zhou and J. S. Luo (private communication).
[19]A. Michalke, J. Fluid Mech. **23**, 521 (1965).
[20]P. A. Monkewitz, to appear in J. Fluid Mech.
[21]A. Michalke, Prog. Aerosp. Sci. **12**, 213 (1972).
[22]C. M. Ho and P. Huerre, Annu. Rev. Fluid Mech. **16**, 365 (1984).

THE FOURTH ASIAN CONGRESS OF FLUID MECHANICS

August 19-23, 1989 Hong Kong

ENTRAINMENT OF 3-D SHEAR LAYERS

C. M. Ho, T. Austin and J. Hertzberg

Department of Aerospace Engineering
University of Southern California
Los Angeles, California 90089-1191

ABSTRACT In engineering devices involving chemical reaction, it is important to be able to control the mass transfer between two streams of fluids. Ho and Gutmark [1] used a small aspect ratio elliptic jet which can significantly enhance the entrainment. This efficient passive control technique is due to the unsteady deformation of 3-D vortical structures caused by self-induction.

1. Passive and Active Control of Free Shear Layers

The possibility of controlling the mass transfer in the transverse direction of a shear layer is important in improving the efficiency of devices with chemical reaction. In a two-dimensional flow, the coalescense of the vortical structures in the shear layer was identified to be the main entrainment mechanism [2]. If the vortex merging is prohibited, the growth of the mixing layer is stopped or even decreased [3]. On the other hand, if the shear layer is actively perturbed by the subharmonics of the most amplified frequency, multiple vortices will merge simultaneously [4]. The growth of the shear layer is increased.

The spatial development of the shear layer is extremely sensitive to the initial perturbations or the boundary conditions. The alternative approach of controlling the enhancement is to change the upstream boundary condition of the shear layer. Ho and Gutmark [1, 5] found that a jet with an elliptic nozzle can entrain much more fluid than that of a circular or a plane jet [Fig. 1]. This passive control method is even more advantageous for engineering applications, because no delicate forcing arrangement is required. More importantly, they identified a new entrainment mechanism; the self-induction of an elliptic vortex ring makes the structure switch its axis orientation, the vortex element near the minor axis moves outward and makes a large amount of ambient fluid move into the jet near the minor axis region. This concept can be generalized and used in other flow configurations, such as combustion chamber.

2. Applications in Combustion

The ramjet is a device which can be benifited by the entrianment contol technique. There is a short distance from the flame holder to the exhaust nozzle. Combustion needs to be accomplished during a short residence time and combustion

instability has been a troublesome problem. The advantages of using an elliptic jet in the ramjet has been shown to be phenomenal. Schadow et al. [6] used a 3:1 elliptical nozzle in a jet with combustion. They found that the centerline temperature increased sharply a short distance from the elliptic nozzle. At the end of the jet potential core, the temperature
was much higher than that of a circular jet [Fig. 2].

The combustion instability problem was alivated by using another type of asymmetric nozzle. They used a triangular nozzle and injected fuel near the tips of the triangle [7]. In this way, the fuel is mixed by the small eddies near the tips and the large structures do not trigger the combustion instability.

3.Supersonic Asymmetric Jet

The spreading rate of a supersonic shear layer is much slower than that of a subsonic flow and the combustion efficiency of supersonic flame is hindered by the low mixing rate. Actually, this is the most pressing problem in developing a hypersonic aircraft. In a preliminary experiment, we found that the small aspect ratio rectangular nozzle could enhance the entrainment as it did in the subsonic flow [8].

In general, the supersonic flows spread slower than that of subsonic flows. However, the entrainment improvement of the rectangular nozzle over the circular nozzle is about the same for both supersonic and subsonic jets in the far downstream locations. Near the Nozzle, the variations of the cross-section area ratios, indicating the shear layer spreading, are similar for supersonic and subsonic cases. Hence, we expect that the supersonic rectangular jet will entrain more mass than that of a supersonic circular jet in the region near the nozzle.

4.Asymmetric Jet in Confinement

Most of the combustion is taking place inside a confined space. The entrainment process is very different from a shear layer in the free space. As has been pointed out in our previous findings [1] the unsteady evolution of the vortex structures can engulf the fluids into the mixing region. We used a 2:1 aspect ratio rectangular jet in a confined environment. The deformation of the vortical structures was found to be much more convoluted than those in a free jet. These deformations are produced by the local 3-D shear layer and the induction of the image vortex. In other words, a properly designed confinement should be able to facilitate the mixing process.

References

[1] Ho, C.M. & Gutmark, E. : J. Fluid Mech. 179, 383 (1987).

[2] Winant, C.D. & Browand, F.K. : J. Fluid Mech. 63, 237 (1974).
[3] Oster, D. & Wygnanski, I. : J. Fluid Mech. 123, 91 (1982).

[4] Ho, C.M. & Huang, L.S. : J. Fluid Mech. 119, 443 (1982).
Jou, W.H., Knoke, G.S. & Ho, C.M. : DOE Ejector Conf. (1988).

[5] Ho, C.M. & Gutmark, E. : Bull. Am. Phys. Soc. 27, 1184 (1982).

[6] Schadow, K.C., Wilson, K.J., Lee, M.J. & Gutmark, E. : AIAA paper No. 84-1260, (1984).

[7] Schadow, K.C., Gutmark, E., Parr, T.P., Parr, D.M., & Wilson, K.J. : JANNAF Combustion Conf. (1986).

[8] Jou, W.H., Knoke, G.S. & Ho, C.M. : DOE Ejector Conf. (1988).

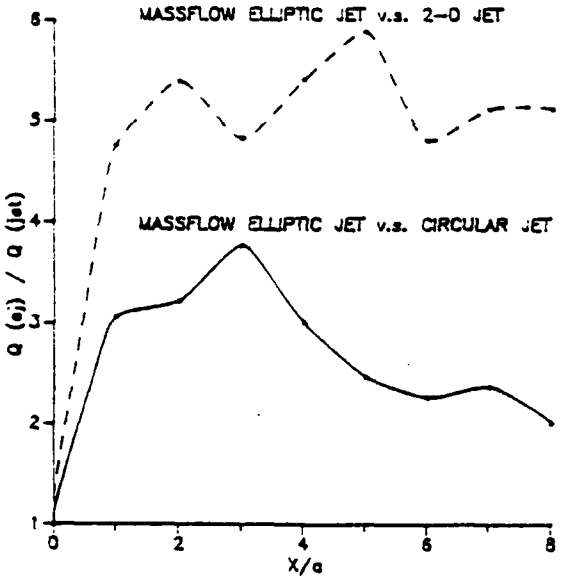

Fig. 1 Mass entrainment rate

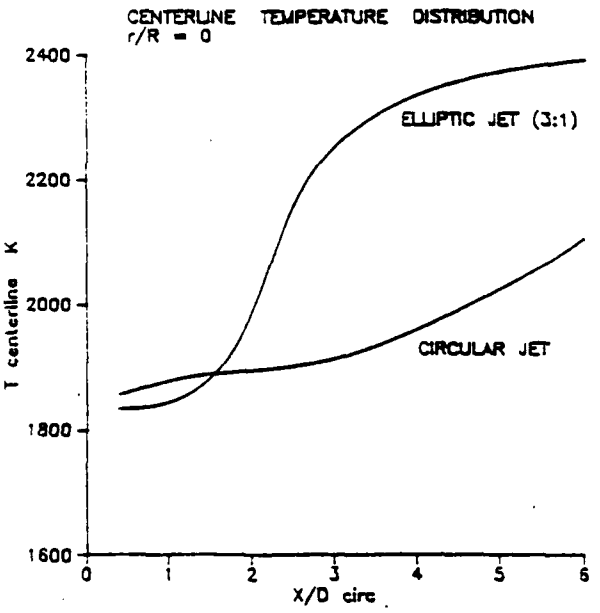

Fig. 2 Centerline temperature

SEARCH FOR CHAOS IN FREE SHEAR FLOWS
THE CASE OF THE WAKE-SHEAR LAYER
(Task 3)

Co-Principal Investigators: L. G. Redekopp, P. Huerre, and C.-M. Ho

STATUS OF RESEARCH EFFORT

1 Local and Global Instabilities

Many flows of technological interest such as jets, wakes, mixing layers, boundary layers, etc. are spatially-developing (i.e., the mean velocity profile is non-uniform in the streamwise direction). In the past three years, we have been able to develop a general theoretical framework to describe these flows from a hydrodynamic stability perspective. The status of recent theoretical and experimental efforts by our group and other teams has been reviewed in [15] (numbers in brackets refer to respective publications listed at the end of the report). Our approach differs markedly from previous work: instead of examining the spatial development of downstream-going waves at a given external real frequency, we argue that one must first determine the absolute/convective nature of the local instability at each streamwise station. If the entire flow is locally convectively unstable, as in spatial mixing layers, boundary layers, constant-density jets, flat-plate wakes, etc., the classical method mentioned above is appropriate. However, when a sufficiently large region of absolute instability exists within the flow domain, as in bluff body wakes, low density jets, capillary jets, etc., one must resort to a global mode description which includes upstream and downstream-going waves of unknown complex frequency. The global mode frequency and its spatial structure are then obtained by solving an eigenvalue problem in the streamwise direction.

Simplified amplitude evolution models, such as the Ginzburg-Landau equation, have proved to be extremely useful to test these new theoretical concepts. We have shown on these models that the onset of global instability results from a well-defined sequence of bifurcations [2,6]. Detailed stability analyses of wakes behind bluff bodies have confirmed that the same scenario is observed experimentally in bluff-body wakes [7,8]. The effects of forcing on global mode dynamics have also been studied on the basis of simplified models: it has been demonstrated that the optimal station for the excitation of global modes is located well upstream of the point of maximum absolute growth rate [4,11]. Furthermore, the application of a forced evolution model to the description of the preferred mode in homogeneous jets has led to surprisingly good results: the predicted Strouhal number of 0.225 compared very favorably with the measured value of 0.25 [11,3]. This led us to conclude that the preferred mode in jets is a weakly-damped global mode which is selectively destabilized by extremely low levels of external noise. Finally, a study of the secondary instabilities arising in some amplitude equations has indicated that primary and secondary instabilities may have a distinct absolute/convective character within the same flow [1].

As briefly alluded to earlier, hydrodynamic stability calculations of wake profiles [7,8] have also been carried out to determine whether absolute/convective instability concepts are

pertinent in real flows. These studies have revealed that a region of local absolute instability exists in the near wake behind bluff bodies when the Karman vortex street is self-sustained. As the Reynolds number is decreased below critical, the absolutely unstable region persists, but it is too small to lead to a self-sustained global mode. In this case, the flow may be locally unstable, but there is no spatially-coherent, temporally-periodic structure characteristic of the Karman vortex street.

A much closer link between local and global properties has been established within the WKBJ approximation for a general class of partial differential equations in one spatial dimension [9,10]. Rigorous mathematical results have been derived. In particular, a simple frequency selection criterion has been proposed: the global mode frequency is given by the value of the absolute frequency $\omega_0(X_s)$ at the stationary point X_s such that $(d\omega_0/dX)_{X_s} = 0$. This provides an explicit relationship between global and local characteristics. It is striking that the global frequency only involves a single streamwise location in the complex X-plane.

2 Spatial chaos: model studies

In convectively unstable flows, interactions between different modes lead to a radically distinct type of dynamics. In contrast with absolutely unstable flows, one expects a great sensitivity to external perturbations. We have conducted an asymptotic study of the interaction between the sinuous and varicose modes in wake-shear layers when the critical layer is dominated by viscous effects [5]. The complex amplitudes of each mode have been shown to be governed by a system of coupled subharmonic resonance equations. A numerical investigaton of the resulting dynamical system has revealed a great variety of possible spatial vorticity distributions as the forcing frequency is gradually increased. In all cases the flow is time periodic but spatial chaos can be generated for specific ranges of forcing frequencies. The nature of the spatial disorder is highly intermittent: the sinuous mode dominates the evolution but localized bursts of the varicose mode occur randomly in space. This intermittency has been used to advantage to derive an analytical one-dimensional map relating successive peaks of the varicose mode.

3 Spatial chaos: experimental studies

3.1 The water channel

The wake-shear layer water channel was assembled and preliminary testing occurred during the current contract period. The facility has a splitter plate which divides the stagnation and contraction sections allowing control of the two independent streams which merge downstream of the splitter plate in the test section. A major modification of the trailing edge of the splitter plate was necessary after early tests revealed that local separation caused a high level of random disturbances. The original trailing edge was made of fiberglass and the tapper angle was larger than prescribed in the original design. We have replaced the last section of the splitter plate with a trailing edge made of precision machined brass. The local separation problem was found to be eliminated. The speeds in the streams on both sides of the splitter plate can be independently controlled for flow speeds up to 1 ft/sec.

Suction or blowing from the trailing edge is also possible to provide independent control of the wake component of the velocity profile for the purpose of investigating various types of instabilities and mode interactions.

3.2 Instrumentation

A powerful new type of instrument, a Particle Displacement Image Velocimeter (PDIV), will be used to measure the velocity field. The PDIV instrument provides a measurement of several thousands of velocity vectors at one time. With this capability, it is possible to investigate the spatial chaos problem in that the instantaneous spatial structure of the velocity field can be obtained as a function of time.

All components of the PDIV system have been received. We experienced a problem with the SUN computer which was subsequently found to arise from an incompatible disk controller. Fortunately, we managed to resolve this problem in the first week of December. The whole system is now functioning and should be in operating condition by January.

3.3 Experimental Results

When both streams have the same speed, a wake flow is produced downstream of the trailing edge of the splitter plate. The arrangement of coherent structures was observed to be of the Karman vortex street type. They were counter-rotating and asymmetrically placed. When the velocity difference between the two streams was increased, a mixing layer eventually formed. All the structures rotated in the same direction. There must be a velocity-ratio range such that both the Karman mode and the mixing-layer mode compete. We placed a pulsed hydrogen bubble wire in the flow and visualized the vortex patterns from the streak lines. When the velocity ratio is close to zero (i.e., strong wake influence), the vortices shifted from the wake type to the mixing layer type intermittently. Whenever, the wake type vortices prevailed, the thickness of the sheared region increased. A hot-film probe was used to measure the passage frequency of the vortices. Based on the time-averaged spectrum, only one peak could be identified. In other words, the flow was temporally periodic, but the vortex arrangement exhibited significant spatial variability. We further found that the phenomenon described above only occurred over a very narrow range of velocity ratios.

PUBLICATIONS

1. Huerre, P. "On the Absolute/Convective Nature of Primary and Secondary Instabilities", In "Propagation in Far From Equilibrium Systems", ed. J. E. Wesfreid et al., pp. 340–353, Berlin, Springer-Verlag, 1988.

2. Chomaz, J. M., Huerre, P. and Redekopp, L. G., "Models of Hydrodynamic Resonances in Separated Shear Flows", *Proceedings of the Sixth Symposium on Turbulent Shear Flows*, Toulouse, France, September 7–9, 1987, pp. 3.2 1–6.

3. Monkewitz, P. A., Huerre, P. and Chomaz, J. M., "Preferred Modes in Jets and Global Instabilities", *Bulletin of the American Physical Society*, Vol. 32, p. 2051, 1987.

4. Chomaz, J. M., Huerre, P. and Redekopp, L. G., "Sensitivity of External Excitations, Absolute and Convective Instabilities in Spatially-Developing Systems", *Bulletin of the American Physical Society*, Vol. 32, p. 2071, 1987.

5. Saulière, J. and Huerre, P., "Spatial Chaos and Nonlinear Interactions in Wake-Shear Layers", *Bulletin of the American Physical Society*, Vol. 32, p. 2071, 1987.

6. Chomaz, J. M., Huerre, P. and Redekopp, L. G., "Bifurcations to Local and Global Modes in Spatially-Developing Flows", *Physical Review Letters*, Vol. 60, pp. 25–28, 1988.

7. Monkewitz, P. A. and Nguyen, L. N., "Absolute Instability in the Near-Wake of Two-Dimensional Bluff Bodies", *Journal of Fluids and Structures*, Vol. 1, pp. 165–184, 1987.

8. Monkewitz, P. A., "The Absolute and Convective Nature of Instability in Two-Dimensional Wakes at Low Reynolds Numbers", *Physics of Fluids*, Vol. 31, pp. 999–1006, 1988.

9. Huerre, P., Chomaz, J. M. and Redekopp, L. G., "A Frequency Selection Criterion in Spatially Developing Flows", *Bulletin of the American Physical Society*, Vol. 33, p. 2283, 1988.

10. Djordevic, V. D. and Redekopp, L. G., "Linear Stability Analysis of Nonhomentropic, Inviscid Compressible Flows", *Phys. Fluids*, Vol. 31, pp. 3239–3245, 1988.

11. Pavithran, S. and Redekopp, L. G., "The Absolute-Convective Transition in Subsonic Mixing Layers", *Phys. Fluids A*, Vol. 1, pp. 1736–1739, 1989.

12. Djordjevic, V. D. and Redekopp, L. G., "Nonlinear Stability of Subsonic Mixing Layers with Symmetric Temperature Variations", *Proc. Roy. Soc. London, Series A*, Vol. 426, pp. 287–330, 1989.

13. Chomaz, J. M., Huerre, P. and Redekopp, L. G., "A Frequency Selection Criterion in Spatially Developing Flows", accepted for publication in *Studies in Appl. Math.*

14. Chomaz, J. M., Huerre, P. and Redekopp, L. G., "Effect of Nonlinearity and Forcing on Global Modes", In Proceedings of "New Trends in Nonlinear Dynamics and Pattern-forming Phenomena. The Geometry of Nonequilibrium". ASI Series B, eds. P. Coullet and P. Huerre. Plenum, New York/London, (in press).

15. Huerre, P. and Monkewitz, P. A., "Local and Global Instability in Spatially Developing Flows", *Annual Rev. Fluid Mech.*, Vol. 22, pp. 473–537, 1990.

INVITED TALKS

1. "Dynamique des Structures Cohérentes et Ondes d'Instabilité dans les Ecoulements Cisaillés", P. Huerre, Special Seminar, Université d'Orsay, Paris, France, September 11, 1987.

2. Spatio-Temporal Dynamics in Free Shear Flows", Invited Lecture, P. Huerre, 40th Annual Meeting of the Division of Fluid Dynamics, American Physical Society, Eugene, Oregon, November 24, 1987.

3. "Large-Scale Dynamics in Free Shear Flows", P. Huerre, Nonlinear Science Seminar, University of California, Santa Barbara, January 22, 1988.

4. "Local and Global Evolution of Instability Waves in Free Shear Flows, P. Huerre, Fluid Mechanics Seminar, California Institute of Technology, Pasadena, January 29, 1988.

5. "Local and Global Evolution of Instabilities in Free Shear Flows", P. Huerre, Seminar in Fluid Dynamics, University of California, San Diego, February 23, 1988.

6. "Global Instability and Chaos in Free Shear Flows", P. Huerre, Department of Mechanical and Materials Engineering Seminar, Washington State University, Pullman, March 9, 1988.

7. "Spatial Chaos and Sensitivity to Forcing in Wake Shear Layers", J. Saulière, Special Seminar, Department of Aerospace Engineering, University of Southern California, April 8, 1988.

8. "Tutorial on Convective and Absolute Instability", P. Huerre, Center for Turbulence Research Summer Program, NASA Ames/Stanford University, Stanford, California, July 6, 1988.

9. "Global Modes in Spatially-Developing Flows", L.G. Redekopp, NATO Advanced Research Workshop on "New Trends in Nonlinear Dynamics and Pattern-Forming Phenomena: The Geometry of Nonequilibrium", Institut d'Etudes Scientifiques de Cargise, Corsica, France, August 2-12, 1988.

10. "Structures Cohérentes et Ondes d'Instabilité dans les Ecoulements Cisaillés", P. Huerre, Seminar, Département de Méchanique, Ecole Polytechnique, Palaiseau, France, December 21, 1988.

11. "Hydrodynamic Instabilities in Free Shear Flows: Spatio-Temporal Descriptions", P. Huerre, Invited Lectures, DARPA/URI Winter School in Fluid Dynamics, Institute for Nonlinear Science, University of California, San Diego, January 9–11, 1989.

12. "Absolute/Convective Instability and Global Modes in Spatially-Developing Flows", P. Huerre, AIAA 2nd Shear Flow Control Conference, Tempe, Arizona, March 13–16, 1989.

13. "Absolute/Convective Instabilities and Global Resonances in Spatially-Developing Flows", P. Huerre, Invited Lecture, March Meeting of the American Physical Society, St. Louis, Missouri, March 21, 1989.

14. "Nature of Bluff-Body Near-Wake Instabilities", P. Huerre, Lead-off Talk, ONR Accelerated Research Initiative on bluff body wake dynamics, Lehigh University, Pennsylvania, May 23, 1989.

15. Open Flow Instabilities", P. Huerre, Invited Lecture, Sixth Taylor-Vortex Flow Working Party, Université Libre de Bruxelles, Bruxelles, Belgium, May 30, 1989.

PROFESSIONAL PERSONNEL

Dr. C. M. Ho: Co-Principal Investigator.
Dr. P. Huerre: Co-Principal Investigator.
Dr. L. G. Redekopp: Co-Principal Investigator.
Dr. M. Rossi: Research Associate.
Ms. D. Wallace: Research Assistant.
Mr. G. Vance: Research Assistant.